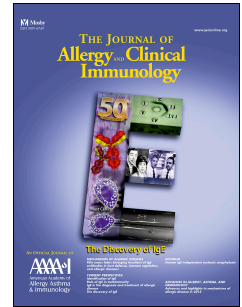


Accepted Manuscript

SLC9A3/NHE3 dysregulation and dilated intercellular spaces in eosinophilic esophagitis

Chang Zeng, B Sc, Simone Vanoni, PhD, David Wu, PhD, Julie M. Caldwell, PhD, Justin C. Wheeler, MD, Kavisha Arora, PhD, Taeko K. Noah, PhD, Lisa Waggoner, B Sc, John A. Besse, B Sc, Amnah N. Yamani, B Sc, Jazib Uddin, B Sc, Mark Rochman, PhD, Ting Wen, PhD, Mirna Chehade, MD, Margaret Collins, MD, Vincent Mukkada, MD, Philip Putnam, MD, Anjaparavanda P. Naren, PhD, Marc E. Rothenberg, MD PhD, Simon P. Hogan, PhD



PII: S0091-6749(18)30633-X

DOI: [10.1016/j.jaci.2018.03.017](https://doi.org/10.1016/j.jaci.2018.03.017)

Reference: YMAI 13409

To appear in: *Journal of Allergy and Clinical Immunology*

Received Date: 28 August 2017

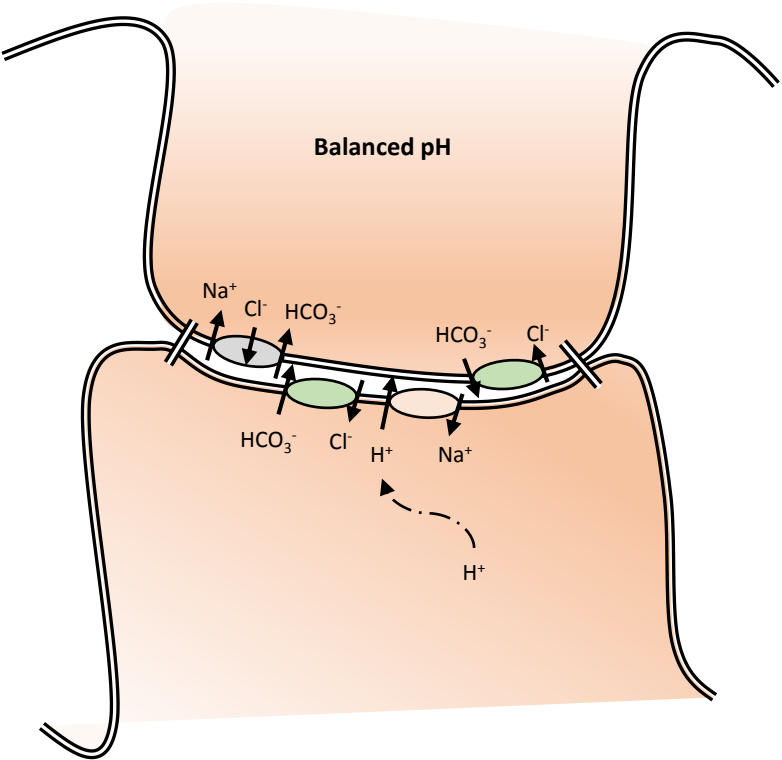
Revised Date: 15 March 2018

Accepted Date: 26 March 2018

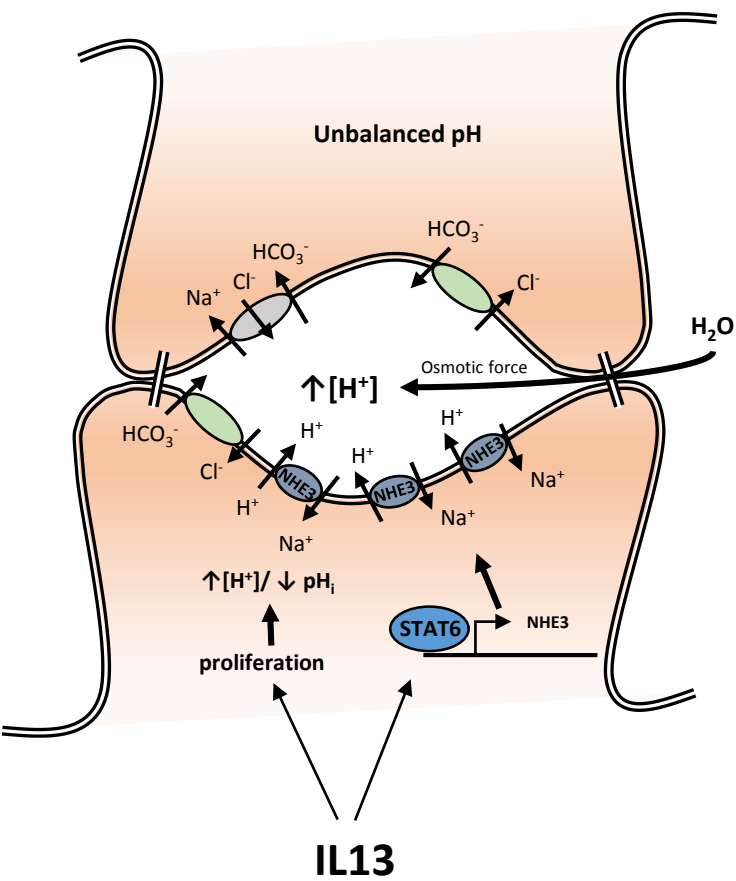
Please cite this article as: Zeng C, Vanoni S, Wu D, Caldwell JM, Wheeler JC, Arora K, Noah TK, Waggoner L, Besse JA, Yamani AN, Uddin J, Rochman M, Wen T, Chehade M, Collins M, Mukkada V, Putnam P, Naren AP, Rothenberg ME, Hogan SP, *SLC9A3/NHE3 dysregulation and dilated intercellular spaces in eosinophilic esophagitis*, *Journal of Allergy and Clinical Immunology* (2018), doi: 10.1016/j.jaci.2018.03.017.

This is a PDF file of an unedited manuscript that has been accepted for publication. As a service to our customers we are providing this early version of the manuscript. The manuscript will undergo copyediting, typesetting, and review of the resulting proof before it is published in its final form. Please note that during the production process errors may be discovered which could affect the content, and all legal disclaimers that apply to the journal pertain.

Normal Stratified squamous esophageal epithelial cells



EoE Stratified squamous esophageal epithelial cells



SLC9A3/NHE3 dysregulation and dilated intercellular spaces in eosinophilic esophagitis

Chang Zeng B Sc¹, Simone Vanoni PhD^{1,5}, David Wu PhD¹, Julie M. Caldwell PhD¹, Justin C. Wheeler MD³, Kavisha Arora PhD², Taeko K. Noah PhD¹, Lisa Waggoner B Sc¹, John A. Besse B Sc¹, Amnah N. Yamani B Sc¹, Jazib Uddin B Sc¹, Mark Rochman PhD¹, Ting Wen PhD¹, Mirna Chehade MD⁶, Margaret Collins MD³, Vincent Mukkada MD⁴, Philip Putnam MD⁴, Anjaparavanda P. Naren PhD², Marc E. Rothenberg MD PhD¹ and Simon P. Hogan PhD^{1,7}

¹Division of Allergy and Immunology, ²Division of Pulmonary Medicine, ³Division of Pathology and Laboratory Medicine, ⁴Division of Gastroenterology, Nutrition and Hepatology, Cincinnati Children's Hospital Medical Center, 3333 Burnet Ave, Cincinnati, OH, 45229; ⁵Institute of Pharmacology and Toxicology, Paracelsus Medical University, Salzburg, Austria. ⁶Mount Sinai Center for Eosinophilic Disorders, Jaffe Food Allergy Institute, Icahn School of Medicine at Mount Sinai, New York, NY. ⁷Department of Pathology, Mary H Weiser Food Allergy Center, Michigan Medicine, University of Michigan, 109 Zina Pitcher Place, Ann Arbor, MI 48109-2200.

Running title: SLC9A3-DIS in Eosinophilic Esophagitis

Grant support: This work was supported by NIH DK090119, NIH AI112626, FARE and The Crohn's Colitis Foundation of America (S.P.H).

Abbreviations: Eosinophilic esophagitis (EoE); dilated intercellular spaces (DIS); interleukin (IL); desmoglein-1 (DSG-1); leucine-rich repeat-containing protein 31 (LRRRC31); kallikrein (KLK); calpain 14 (CAPN14); gastroesophageal reflux disease (GERD); RNA sequencing (RNAseq); solute carrier family (SLC); solute carrier family 9, subfamily A, member 3 (SLC9A3); sodium-hydrogen exchanger member 3 (NHE3); primary esophageal epithelial cells (ESSE); tumor necrosis factor (TNF); interferon (IFN); Signal transducer and activator of transcription (STAT); gamma-interferon-activation site (GAS); epidermal growth factor (EGF); platelet derived growth factor (PDGF); carbonic anhydrases (CA2); basal zone hyperplasia (BZH)

Correspondence: Simon P. Hogan, PhD, Department of Pathology, Mary H Weiser Food Allergy Center, Michigan Medicine, University of Michigan, 109 Zina Pitcher Place Ann Arbor, MI 48109-2200; Email: sihogan@med.umich.edu; Phone: 734-647-9923.

Disclosures: M.E.R. is a consultant for Immune Pharmaceuticals, NKT Therapeutics, Pulm One, Celgene, Shire, GlaxoSmith Kline, Astra Zeneca and Novartis and has an equity interest in the first three companies listed and royalties from reslizumab (Teva Pharmaceuticals). M.E.R. is an inventor of several patents, owned by Cincinnati Children's, and a set of these patents relates to molecular diagnostics. M.C. is a consultant for Shire and Actelion and has received research grant support from Shire, Regeneron and Nutricia. The other authors have declared that they have no conflict of interest.

Abstract

Background: Eosinophilic esophagitis (EoE) is characterized by histopathologic modifications of esophageal tissue including eosinophil-rich inflammation, basal zone hyperplasia (BZH) and dilated intercellular spaces (DIS). The underlying molecular processes that drive the histopathologic features of EoE remain largely unexplored.

Objective: To investigate the involvement of SLC9A3 in esophageal epithelial $[pH]_i$ and DIS formation and the histopathological features of EoE.

Methods: We examined expression of esophageal epithelial gene networks associated with regulation of intracellular pH ($[pH]_i$) in the EoE transcriptome of primary esophageal epithelial cells and an in vitro esophageal epithelial 3D model system (EPC2-ALI). Molecular and cellular analyses and ion transport assays were employed to evaluate expression and function of SLC9A3.

Results: We identified altered expression of gene networks associated with regulation of intracellular pH ($[pH]_i$) and acid protective mechanisms in esophageal biopsies from pediatric patients with EoE (normal $n = 6$, EoE $n = 10$). The most dysregulated gene central to regulating $[pH]_i$ was *SLC9A3*. *SLC9A3* expression was increased within the basal layer of esophageal biopsies from patients with EoE and that expression positively correlated with disease severity (eosinophils/HPF) and DIS (normal $n = 10$, EoE $n = 10$). Analyses of esophageal epithelial cells revealed IL-13–induced, STAT6-dependent *SLC9A3* expression and Na^+ -dependent proton secretion and that *SLC9A3* activity positively correlated with DIS formation. Finally, we showed that IL-13–mediated Na^+ -dependent proton secretion was the primary intracellular acid protective mechanism within the esophageal epithelium and that blockade of *SLC9A3* transport abrogated IL-13–induced DIS formation.

Conclusions: *SLC9A3* plays a functional role in DIS formation and pharmacologic interventions targeting *SLC9A3* function may suppress the histopathologic manifestations in EoE.

Short Summary

IL13-induced SLC9A3/NHE3 upregulation in Eosinophilic Esophagitis leads to increased intracellular pH, and contributes to the dilated intercellular spaces (DIS) formation.

Key Messages

- EoE transcriptome consists of altered expression of gene networks associated with regulation of intracellular pH ($[pH]_i$) and acid protective mechanisms.
- Increased expression of levels of *SLC9A3* within the basal layer of esophageal biopsies from patients with EoE and that expression positively correlated with disease severity (eosinophils/HPF) and DIS.
- IL-13–induced *SLC9A3* expression and Na^+ -dependent proton secretion and that *SLC9A3* activity positively correlated with DIS formation.
- IL-13–mediated Na^+ -dependent proton secretion was the primary intracellular acid protective mechanism within the esophageal epithelium.
- *SLC9A3*-dependent transport is required for IL-13–induced DIS formation.

Key Words

SLC9A3/NHE3; ion transport; Eosinophilic Esophagitis; Dilated intercellular spaces (DIS); IL-13.

Introduction

Eosinophilic esophagitis (EoE) is a food allergen-induced inflammatory disease that is increasing in incidence (5 – 10 cases per 100,000) and prevalence (0.5 to 1 case per 1000)¹⁻⁴. Common symptoms of EoE include vomiting, dysphagia, chest pain, food impaction and upper abdominal pain⁵ and decrease the health-related quality of life⁶.

Corroborative clinical and experimental studies indicate that an underlying allergic sensitization to dietary food antigens and development of a CD4⁺ Th2 and ILC2 inflammatory response in the esophageal mucosa drive the eosinophilic inflammation and esophageal remodeling in EoE, which includes basal zone hyperplasia (BZH) and dilated intercellular spaces (DIS)⁷⁻¹⁰. Dietary modification (i.e., complete or targeted food antigen avoidance) and swallowed glucocorticoids alleviate much of the disease pathology^{11, 12}, suggesting a food-induced CD4⁺ Type-2 allergic inflammatory response¹³⁻¹⁸. Consistent with this, animal-based studies have revealed important roles for CD4⁺ Th2 cells, pro-allergic cytokines [interleukin 5 (IL-5), IL-13] and eosinophils in the histopathologic manifestations of disease¹⁹⁻²¹. One cytokine that seems to be central in orchestrating the EoE phenotype is IL-13²²⁻²⁴. IL-13 is highly upregulated in the esophageal tissue of patients with EoE and is sufficient to alter gene expression in esophageal epithelial cells in vitro and in vivo, and the IL-13-induced transcriptome significantly overlaps with the transcriptional changes observed in esophageal biopsies of patients with EoE²²⁻²⁴. Importantly, treating patients with EoE with a humanized antibody against IL-13 led to a significant decrease in esophageal eosinophil count and had a normalizing effect on the dysregulated transcriptome observed in patients with EoE²⁵. IL-13 has been shown to dysregulate the expression of several key epithelial barrier regulatory genes including desmosomal cadherin, desmoglein-1 (DSG-1), leucine-rich repeat-containing protein 31 (LRRC31), kallikrein (KLK) serine proteases and calpain 14 (CAPN14), which have been linked with EoE²⁶⁻²⁸.

Though there have been significant advances in our understanding of a link between allergic inflammation and EoE, there is a paucity of data revealing the underlying pathways that regulate epithelial BZH and DIS in EoE. DIS, also described as

spongiosis, is a morphologic feature that has been identified in multiple forms of esophagitis including lymphocytic esophagitis²⁹, gastroesophageal reflux disease (GERD)³⁰ and EoE^{8, 31}. Histologic comparison between GERD and EoE suggested that DIS is significantly more intense in EoE than GERD³². Steroid therapy or elimination diet significantly decreases DIS in patients with EoE, and this decrease is associated with improvement of patients' symptoms³¹, indicating an association between DIS and the etiology of EoE. The underlying molecular pathways that drive DIS formation are currently unknown.

We recently performed RNA sequencing (RNAseq) on esophageal mucosal biopsies from normal healthy control patients (NL) and patients with active, proton pump inhibitor (PPI)–confirmed EoE. We identified a total of 1607 significantly dysregulated transcripts (1096 upregulated, 511 downregulated), with 66% of the gene signature being similar to the EoE transcript signature identified by microarray-based expression profiling²⁴. We have performed gene ontology enrichment network analysis of the 1607 significantly dysregulated transcripts and identified dysregulation of transmembrane transporter activity genes associated with regulation of $[pH]_i$ and acid protective mechanisms. The most dysregulated transmembrane transporter activity gene in the EoE transcriptome was the solute carrier family 9, subfamily A, member 3 (*SLC9A3*), which encodes sodium-hydrogen exchanger member 3 (NHE3)³³ (33-fold increase). We demonstrate a significant increase of *SLC9A3* in the esophageal epithelium in two independent, confirmatory patient cohorts with PPI-confirmed EoE. We show that the expression level of NHE3 positively correlated with the level of inflammation and the area of DIS. IL-13 treatment of esophageal epithelial primary cells derived from patients with EoE and in a differentiated squamous esophageal epithelium model (EPC2-ALI) increased NHE3 expression and ion transport activity. Pharmacologic inhibition of NHE3 function substantially decreased the area of IL-13–induced DIS. These collective data suggest that increased expression and activity of NHE3 contribute to the formation of DIS in the esophageal epithelium in EoE.

Material and Methods

Human subjects. NL (healthy control patients) were defined as having no history of EoE diagnosis, 0 esophageal eosinophils per high-power field (HPF) and no evidence of esophagitis within distal esophageal biopsies obtained during the same endoscopy procedure as the analyzed samples. EoE was defined as described in the recent consensus guidelines. Specifically, patients needed to have ≥ 15 eosinophils in at least 1 high-power field (eos/hpf) in a distal esophageal biopsy with other causes of esophageal eosinophilia excluded, and without a response to acid suppression. Normal control patient cohort consists of patients with a variety of non-specific upper GI complaints including vomiting, loose stools, abdominal pain, nausea who underwent endoscopy were biopsied and demonstrated to have no histological evidence of esophageal disease. RNAseq and validation qRT-PCR analyses and histology (Eos/hpf and DIS quantification) studies were performed on the esophageal biopsies. RNAseq and qRT-PCR analyses and histology (Eos/hpf and DIS) were performed on human esophageal biopsy samples (normal, n = 6; EoE, n = 10) as previously described (NCBI Gene Expression Omnibus (GEO) database under accession GSE58640)²⁴ (Cohort 1). The demographics of the normal control and EoE patients are described in Supplemental Figure S1. The qRT-PCR and histopathology (Eos/hpf) analyses was performed on a second independent cohort (normal, n = 10; EoE, n = 10) (Cohort 2). The demographics of the patients and controls are described in Supplemental Figure S1.

RNA-sequencing of human Biopsy Samples: Esophageal biopsy RNA was isolated from controls and EoE patients with active disease using the RNeasy kit (QIAGEN Incorporated, Germantown, MD) per the manufacturer's protocol. RNA libraries were prepared using standard Illumina protocols (TrueSeq RNA LS Sample Prep V2) at the CCHMC Genetic Variation and Gene Discovery Core. RNA sequencing acquiring 100bp reads from paired end libraries was performed at the Genetic Variation and Gene Discovery Core Facility at CCHMC using Illumina HiSeq 2500. The paired-end sequencing reads were aligned against the GRCh37 genome model using TopHat 2.04 with Bowtie 2.03^{34, 35}. The separate alignments were then merged using

Cuffmerge³⁶ with UCSC gene models as a reference. Raw data were assessed for statistical significance using a Welch t-test with Benjamini-Hochberg false discovery rate and a threshold of $P < 0.05$ and a 2.0-fold cut-off filter in GeneSpring® GX (Agilent Technologies Incorporated, Clara, CA).

RNA-sequencing of mature EPC2-ALI: RNA was isolated using the RNeasy kit (QIAGEN Incorporated, Germantown, MD, USA) per manufacturer instructions. Assessment of RNA quality was performed using the Agilent 2100 Expert bioanalyzer (Agilent Technologies Incorporated, Clara, CA, USA) and only those samples getting a RNA Integrity Number (RIN) above 8 were chosen for sequencing. Next generation sequencing analyses were performed by the CCHMC Genetic Variation and Gene Discovery Core with Illumina HiSeq 2500. Raw data was uploaded on Biowardrobe³⁷ and RPKM values were calculated. Differentially expressed genes were assessed using DEseq2.

Gene Ontology Analysis: Gene list enrichment analysis and candidate gene prioritization based on molecular function using ToppGene³⁸ with FDR B&H correction and p-Value cutoff at 0.05. Heatmaps were generated using RStudio.

Pathology analysis.

Biopsy preparation. Formalin-fixed, paraffin-embedded esophageal biopsies were sectioned into 5- μ m slides. After removal of paraffin and serial hydration, sections were stained with hematoxylin and eosin (H&E). H&E-stained slides were then imaged using an Olympus DP-72 microscope (Olympus Corporation, Semrock, New York, NY, USA).

Quantification of intercellular space. Intercellular space was quantified as the percentage of intercellular area of the total area of the biopsy sample using Image-Pro Plus software (Media Cybernetics, Rockville, MD, USA) automated space measurement function and calculated by the ratio of intercellular area / total tissue area.

qPCR analysis. RNA samples were extracted from esophageal biopsy, cultured primary cells or EPC2-ALI cultures using the RNeasy kit (QIAGEN Sciences Incorporated, Germantown, MD, USA) according to the manufacturer's protocol. Purified RNA (300 – 500 ng) was DNase treated and reverse transcribed to cDNA using Superscript II RNase H Reverse Transcriptase (Thermo Fisher Scientific Incorporated,

Rockford, IL, USA) per the manufacturer's instructions. cDNA for *SLC9A3* and 18S were quantified by real-time PCR using Taqman Universal supermix with the CFX96 Real-Time PCR Detection System. qPCR analysis was performed using the Bio-Rad CFX Manager Software version 3.1. Primers for *SLC9A3* and 18S were purchased from Taqman (Thermo Fisher Scientific, Waltham, MA).

Immunofluorescence (IF) staining. For IF staining, formalin- or paraformaldehyde-fixed, paraffin-embedded esophageal biopsies or EPC2-ALI cultures were sectioned, mounted on slides and de-paraffinized using standard histological procedures. Slides were then permeabilized in Tris-EDTA (1 mM, pH 9.0) with 0.1% Tween-20, and antigen exposure was performed at 125°C for 30 s in a decloaking chamber using a pressure cooker. Slides were then blocked by 10% normal donkey serum for 1 h followed by overnight incubation of primary antibodies diluted in 10% normal donkey serum: NHE3 (Novus, Littleton, CO) and CK13 (Invitrogen, Carlsbad, CA). Slides were then washed and incubated with secondary antibody at room temperature for 1 h. Slides were mounted with Fluoromount-G (SouthernBiotech, Birmingham, AL) mounting solution. Fluorescent imaging was performed using the Zeiss Apotome fluorescent microscope using NIKON elements software.

Primary cell preparation. Distal esophageal biopsy was obtained from NL or EoE patients who underwent routine endoscopy, suspended in 1 mL keratinocyte serum-free media (KSFM) (Invitrogen, Carlsbad, CA) containing supplements [human epidermal growth factor (EGF) (1 ng/mL), bovine pituitary extract (50 µg/mL), and 1X penicillin/streptomycin (Invitrogen, Carlsbad, CA)] and subsequently placed in 60-mm dish in 3 mL of filter-sterilized (0.2 µm) Leibovitz's L-15 media (Invitrogen, Carlsbad, CA) containing 115 U/mL collagenase, 1.2 U/mL dispase and 1.25 mg/mL BSA. The biopsy was mechanically dispersed using scissors to pieces less than 1 mm in size and then incubated at 37°C for 1 h. The cell suspension was centrifuged at 500 g for 5 min at 4°C and the pellet washed twice with 5 mL of supplemented KSFM media. Cells were suspended in 1 mL of 0.05% trypsin/EDTA for 10 min at 37°C and agitated every 2 min. Trypsin activity was inhibited with soybean trypsin inhibitor (STI) (250 mg/L in 1X DPBS; 5 mLs). Cells were pelleted by centrifugation, suspended in 1 mL KSFM containing

supplements, transferred to a 35-mm dish containing irradiated NIH 3T3 J2 fibroblasts (162,500 cells) and cultured at 37°C and 5% CO₂. Media were changed at day 5 and every other day thereafter using KSFM containing supplements. After epithelial cells became 60-70% confluent, they were dispersed from the plate using 0.05% trypsin/EDTA for 10 min at 37°C and agitated every 2 min. Trypsin digestion was inactivated by STI, and cells were then passaged in KSFM containing supplements at 1-2 x 10⁵ cells per 3 mL in a 60-mm dish.

pH_i assay. Primary esophageal epithelial cells were cultured on Ibidi μ -Slide 4 well (ibidi GmbH, Germany) with a concentration of 25,000 cells/well. After 24 h of equilibration period, cells were stimulated with or without 100 ng/mL recombinant human IL-13 (PeproTech, Rocky Hill, NJ) for another 48 h. pH_i changes in these primary cells were measured with the pH-sensitive fluorescent dye BCECF AM (2',7'-bis-(2-carboxyethyl)-5-(and-6)-carboxyfluorescein, acetoxymethyl ester) or SNARF-5F AM (SNARF-5F 5-(and-6)-carboxylic acid, acetoxymethyl ester) (Invitrogen, Carlsbad, CA). Cells were loaded with 10 μ M BCECF AM or SNARF-5F AM in HCO₃⁻-free Ringer's solution [mM, 110 NaCl, 25 Na-Gluconate, 5 KCl, 0.5 MgSO₄·7H₂O, 1 CaCl₂·2H₂O, 10 HEPES, 4 Glucose; to pH 7.4] at 37°C for 30 min prior to the experiment. To remove the extracellular dye, cells were washed two times with HCO₃⁻-free Ringer's solution at the end of the incubation period. To acidify the intracellular compartment of cells and generate the necessary H⁺ gradient (high [H⁺] inside vs low [H⁺] outside cell) to measure pH_i recovery rate, 20 mM of NH₄Cl was added to the chamber after the first 5-min recording of the baseline pH_i (Figure 2C. Stage II). To measure the Na⁺-dependent pH_i recovery rate, Na⁺ was first removed from the cells by replacing the buffer with Na⁺-free Ringer's solution [mM, 135 NMDG-Cl, 5 KCl, 0.5 MgSO₄·7H₂O, 1 CaCl₂·2H₂O, 10 HEPES, 4 Glucose; to pH 7.4] for 5 min (Figure 2C. Stage III). Na⁺-dependent pH_i recovery rate was measured by replacing extracellular solution to HCO₃⁻-free Ringer's solution containing 135 mM Na⁺ (Figure 2C. Stage IV) and determination of the slope of the Na⁺-dependent pH_i change. The pH_i values are derived from the calibration curves described below. The statistical significance of Na⁺-dependent pH_i change was determined using a Student's t-test (two-tailed). To record the BCECF AM fluorescence change, cells were imaged by a Nikon Spectra X inverted fluorescent microscope with

the excitation wavelength of 512 nm / 440 nm and emission at 535 nm. To record the SNARF-5F AM fluorescence change, cells were imaged by Zeiss LSM710 LIVE DUO confocal microscope with excitation wavelength at 488 nm and the emission wavelength of 640 nm / 580 nm. To inhibit NHE3 activity, 30 μ M of S3226 or 0.01% DMSO (vehicle) was applied throughout the experiment. % S3226-sensitive Na^+ -dependent pH_i recovery rate was calculated as Recovery rate of (DMSO-treated - S3226-treated)*100/DMSO-treated %. Quantification was performed on 10-20 cells randomly picked in each sample, and the fluorescence intensity was measured using Nikon Elements microscope imaging software or ImageJ software. These fluorescence intensity values were then converted into pH values per calibration curves. A calibration curve was generated at the end of each experiment; BCECF AM or SNARF-5F AM intensity was calibrated against pH_i when cells were exposed to the K^+/H^+ ionophore nigericin (10 μ M) and valinomycin (10 μ M) (Invitrogen, Carlsbad, CA) in high- K^+ solution at four different pH values. High- K^+ solution [mM, 20 NaCl, 130 KCl, 1 MgCl_2 , 1 $\text{CaCl}_2 \cdot 2\text{H}_2\text{O}$, 5 HEPES] was prepared and titrated to a pH ranging from 6.5 to 7.9. Fitting was performed with GraphPad Prism software.

EPC2-ALI culture. The hTERT-EPC2 cells (hTERT-immortalized human esophageal keratinocytes) were a kind gift from Dr. Anil Rustgi (University of Pennsylvania, Philadelphia, PA, USA) as previously described³⁹. The air-liquid interface (ALI) culture system was previously described and characterized together with EPC2 cells²⁸. EPC2 cells were grown to fully submerge on 0.4- μ m pore size, permeable transwell inserts (Corning Incorporated, Corning, NY) in KSFM (Life Technologies, Carlsbad, CA, USA). As depicted in Figure 3A, (i) Day 0, cells were seeded on a permeable membrane support and grown to single submerged layer after three days. (ii) Cells were then shifted to medium containing high $[\text{Ca}^{2+}]$ to induce tight junction formation ($[\text{Ca}^{2+}] = 1.8\text{mM}$). (iii) On Day 7, media were removed from top chamber in order to induce differentiation and epithelial stratification in ALI. (iv) Day 12 (5 days post ALI), cells were then treated with vehicle or cytokine (IL-13) in the presence and absence of SLC9A3 inhibitor (30 μ M)⁴⁰ as described in figure legends.

Lentiviral Transduction. EPC2 cells at 60-70% confluence were transduced with lentiviral particles containing Mission[®] STAT6 shRNA TRC 0000019409 shRNA, Mission[®] STAT3 (TRCN0000329887) shRNA (Sigma; St. Louis, MO, USA) or Mission[®] non-target control shRNA (Sigma; St. Louis, MO, USA). All the three shRNA lentivirus were generated by the Cincinnati Children's Hospital Medical Center Viral Core using a 4-plasmid packaging system. Lentiviral particles were incubated with EPC2 cells for 6 hours with a Multiplicity of Infection (MOI) from 0.5 to 10 for STAT3 or CTRL shRNA. For STAT6 shRNA, 10 μ L to 50 μ L viral particles were added to the cells. All the viral particles were added in the presence of 5 μ g/mL Hexadimethrine Bromide (Polybrene[®]) (Sigma; St. Louis, MO, USA). During the first hour of incubation cells were spun down at 1000*g for 1 hour at room temperature. 6 hours following transduction cells were put in fresh KSFM media, and 24 hours later media containing 1 μ g/mL of Puromycin (Thermo Fisher Scientific Incorporated; Rockford, IL, USA) was used for selection. Cells were grown under selective pressure and cultured as regular EPC2 cells. Stable knockdown of STAT6 and STAT3 in EPC2-ALI cultures were evaluated by Western blot. The results indicated an 80% reduction of STAT6 and 90% reduction of STAT3, relatively, compared to empty control transduced cells.

Western blot. EPC2-ALI cultures were lysed using protein lysis buffer (10% Glycerol, 20 mM Tris HCl pH 7, 137 mM NaCl, 2 mM EDTA, 1% NP40 in H₂O) supplemented with Halt protease inhibitor cocktail (Thermo Fisher Scientific Incorporated, Rockford, IL, USA). Proteins were then quantified with BCA assay, and 20 μ g of protein extracted together with protein-reducing buffer was loaded and separated on a 4%-12% Bis-Tris gel and transferred to a nitrocellulose membrane (Life Technologies, Carlsbad, CA). Antibody of NHE3 and α -actin were used for protein detection. The IRDye 800 CW goat anti-rabbit IgG (H+L) (Li-Cor, Lincoln, NE) was used as the secondary antibody for detection. Western Blot quantification was performed using Image Studio Lite (Li-Cor, Lincoln, NE).

pH-STAT assay. Acid secretion by confluent epithelium was quantitated using pH-STAT (TIM856, Radiometer Analytical, Loveland, CO) connected to an Ussing chamber

system as previously described⁴¹. EPC2-ALI cultures were mounted into an Ussing chamber containing unbuffered Ringer's solution [mM, 145 NaCl, 2 KCl, 1 MgCl₂, 2 CaCl₂, 5 Glucose] while gassed with 99.5% oxygen. Both the pH electrode and the titrating burette are placed in the apical side chamber. To measure the equilibrium extracellular pH, without any titration, the extracellular pH was measured for 10 min or until a stable pH was achieved (<0.002 pH unit change/min). After the equilibrium period and extracellular pH measurements were obtained, the mucosal pH was adjusted by titration to a set pH (pH 7.6) to keep the extracellular pH slightly alkalized. Titration rate (amount of alkaline injected by the machine to neutralize the acid secreted by EPC2-ALI culture to maintain the set pH) was used to measure the acid secretion rate.

Histologic analysis for EPC2-ALI. EPC2-ALI cultures were treated as indicated in experiments and then fixed on transwell supports with 4% paraformaldehyde for 1 h at room temperature. Fixed membranes underwent a series of dehydration steps, cleared in HistoClear solution, embedded in paraffin and sectioned into 5- μ m slides. The slides were stained using H&E staining and imaged using an Olympus DP-72 microscope (Olympus Corporation, Semrock, New York, NY, USA).

Electron microscopy. EPC2-ALI cultures were treated as indicated in experiments, fixed with 3% glutaraldehyde and submitted to CCHMC Pathology Research Core for processing, sectioning and transmission electron microscopy using a Hitachi model H-7650 electron microscope, at 80 kV, using the AMT-600 image capture engine software.

Statistical analysis. The statistical significance of EPC2-ALI samples was established using an unpaired t-test (two-tailed), or two-way ANOVA if there were more than one variable. For non-normally distributed data from patient biopsies and primary cells derived from patient biopsies, the Mann-Whitney test was used, and the correlation analyses were assessed with a Spearman correlation test. Graphs and statistical analyses were performed using GraphPad Prism 7.02 (GraphPad Software Incorporated, La Jolla, CA, USA).

Results

Transmembrane transporter *SLC9A3/NHE3* specifically upregulated and correlated with eosinophil count and DIS in EoE

To begin to determine the potential involvement of transmembrane transporter activity in the histopathologic alterations of the esophageal epithelium in EoE, we applied gene ontology (GO) enrichment analysis of the 1607 differentially expressed RNA transcripts identified by RNAseq analyses of pediatric NL and EoE biopsy samples²⁴. GO analysis revealed 50 individual GO nodes significantly dysregulated in the EoE transcriptome based on functional annotations and protein interaction networks (FDR-corrected $p < 0.05$, Supplemental Figure S2). Of these GO nodes, 5 were related to transmembrane transporter activity (Fig. 1A). A combinatory comparison of all 62 genes within these 5 GO nodes revealed that the most upregulated transmembrane transporter activity gene was *SLC9A3*, which encodes for the sodium-hydrogen exchanger family member 3 (NHE3) (Fig. 1B). *SLC9A3* was induced 33-fold in patients with EoE compared to NL (Fig. 1C). In contrast, expression of other members of the *SLC9* family, including the ubiquitously expressed sodium-proton exchanger *SLC9A1*, also referred to as sodium-hydrogen exchanger family member 1 (NHE1), were not dramatically different in expression between EoE and NL (Fig. 1D). Correlation analyses revealed a positive correlation between the level of peak distal esophageal eosinophils and *SLC9A3* expression (Fig. 1E, $r = 0.7167$, $p < 0.05$). Notably, this was specific to *SLC9A3*, as we did not observe any correlation with *SLC9A1* (Fig. 1E, $r = 0.3201$, $p > 0.05$), revealing a specific link between *SLC9A3* expression and disease severity in EoE. To confirm these observations, we examined a second independent pediatric cohort [NL $n = 10$, active EoE $n = 10$] for which we had paired RNA and histologic biopsy samples from the same day of endoscopy. Consistent with our RNAseq analyses, qPCR analyses revealed significant *SLC9A3* overexpression in the pediatric EoE cohort (Fig. 1F). Furthermore, we observed a positive Pearson correlation between *SLC9A3* expression level and distal peak esophageal eosinophil numbers (Fig. 1G, $r = 0.9172$, $p < 0.0001$).

We next performed immunofluorescence (IF) analyses to determine the cellular and spatial expression of NHE3 in NL and EoE esophageal biopsy samples. Consistent with

our RNAseq and PCR analyses, we observed very little expression of NHE3 in healthy esophageal epithelium (Fig. 1H, upper panel). The positive staining observed was restricted to the CK13⁻ single-cell basal esophageal epithelial layer (Fig. 1H, upper panel). In EoE, NHE3 protein expression was remarkably increased, localized to the esophageal basal cell layer and also expanded into the CK13⁺ suprabasal layer (Fig. 1H, lower panel). The localization of NHE3 to the suprabasal zone, an area associated with DIS formation, lead us to examine the relationship between *SLC9A3* expression and DIS in EoE esophageal biopsies. Notably, *SLC9A3*, but not *SLC9A1*, expression positively correlated with the percentage of DIS area in EoE individuals ($r = 0.8095$, $p < 0.05$) (Fig. 1I). These cumulative data indicate a specific upregulation of *SLC9A3*/NHE3 in the suprabasal layer of esophageal epithelium in patients with EoE and that *SLC9A3* levels correlate with esophageal eosinophilic inflammation and DIS.

Increased NHE3 function in IL-13–stimulated primary esophageal epithelial cells.

The epithelial sodium-proton exchanger, NHE3, is predominantly expressed in the apical membrane of epithelia and is the principal mechanism for electroneutral exchange of (Apical → Baso) Na⁺ and (Baso → Apical) H⁺ and plays an important role in the maintenance of intracellular pH (pH_i) and regulation of cell volume⁴². Given IL-13's known role in upregulating the EoE transcriptome¹⁸ and that humanized anti-IL-13 monoclonal antibody (QAX576) has been shown to modulate expression of an anion transport activity node²⁵, we examined the impact of IL-13 exposure on *SLC9A3* expression in primary esophageal epithelial cells. We demonstrate upregulation of *SLC9A3* expression in primary esophageal epithelial cells following IL-13 stimulation (Fig. 2A). To determine whether increased *SLC9A3* expression was associated with altered NHE3 activity, we examined the effect of IL-13 exposure on intracellular pH ([pH]_i) in primary esophageal epithelial cells. Notably, increased *SLC9A3* expression coincided with a significant increase in baseline pH_i (Fig. 2B) and Na⁺-dependent pH_i recovery rate (Fig. 2C-D), supporting an overall increase of Na⁺/H⁺ exchange activity. Notably, the recovery rate positively correlated with *SLC9A3* expression in primary esophageal epithelial cells ($r = 0.9503$ $p < 0.01$; Fig. 2E), suggesting that the increase of pH_i recovery rate in IL-13–treated primary esophageal epithelial cells is predominantly due to increased NHE3 expression. Addition of the NHE3-specific inhibitor S3226 (30

μM) confirmed that the IL-13–induced increase in Na⁺-dependent pH_i recovery rate was predominantly mediated by NHE3 (Fig. 2F).

IL-13 induces an EoE-like transcriptome including increased transmembrane transporter activity and SLC9A3 overexpression in an in vitro, matured esophageal epithelium model system.

In order to define the involvement of SLC9A3/NHE3 in the regulation of [pH]_i and DIS formation in a mature esophageal epithelial model system, we adapted an *in vitro* model developed from keratinocyte esophageal epithelial cells (EPC2) grown in air-liquid interface (ALI)²⁸. EPC2 cells were grown under submerged conditions in low-calcium media (0.09 mM; days 0-3), changed to high-calcium media (1.8 mM, days 3-7) and then exposed to the ALI for 5 days in the presence of high calcium (1.8 mM, days 7-12) to induce differentiation and formation of a mature, stratified epithelium (Fig. 3A). Following maturation, EPC2-ALI cells were stimulated with vehicle or IL-13 and RNAseq analyses performed (Fig. 3A, days 12-14). We show that IL-13 significantly dysregulated a total of 572 genes ($p < 0.05$, fold change > 2.0); notably, many of the most highly dysregulated genes included inflammatory genes associated with EoE, including *CCL26* (7-fold), *TNFAIP6* (9-fold), *CDH26* (3-fold) and *CAPN14* (5-fold), and also gene families located in the epidermal differentiation cluster (EDC) on chromosome 1q21 (e.g., *IVL*, *LOR*, *S100A4*, *S100A6*) (Fig. 3B and Supplemental Table S1). Consistent with these findings, comparative analyses of the IL-13–induced transcriptome changes in EPC2-ALI cells with that of the EoE-specific transcriptome revealed significant overlap with the EoE-specific transcriptome (Fig. 3B, $p < 0.0001$). GO analysis based on the biological process on IL-13–dysregulated genes revealed the most significant 15 individual GO biological process nodes were associated with keratinization, epidermis development, skin development, keratinocyte differentiation, epidermal cell differentiation and inflammatory response and GO Pathways associated with formation of the cornified envelope, keratinization and interleukin-4 and 13 signaling (Supplemental Table S2, FDR-corrected $p < 0.05$). To examine the effect of IL-13 on transmembrane transporter activity, we performed GO analysis based on the molecular function of the 572 genes and identified 6 nodes significantly dysregulated related to transmembrane transport activity (Fig. 3C, FDR-corrected $p < 0.05$). Of the 28

differentially expressed transmembrane transport activity genes in these 6 GO nodes, *SLC9A3* was one of the most highly upregulated genes (Fig. 3D).

IL-13 is known to signal through the JAK/STAT pathway, in particular through a STAT3- and STAT6-dependent signaling pathway⁴³. To determine the involvement of STAT-3 and STAT-6 in IL-13 induction of *SLC9A3* we examined *SLC9A3* mRNA expression in *STAT3* and *STAT6* shRNA-transduced EPC2-ALI cells following IL-13 stimulation. Notably, STAT-3 knockdown in EPC2-ALI cells caused no significant reduction in IL-13-induced *SLC9A3* expression compared to control shRNA-transduced EPC2-ALI cells (Figure 3E). In contrast, *STAT6* knockdown in EPC2-ALI cells significantly ablated IL-13-induced *SLC9A3* expression (50% reduction), suggesting that IL-13-induced STAT6 signaling is important for *SLC9A3* expression in EPC2-ALI cells (Figure 3E). These studies demonstrate that IL-13 induces *SLC9A3* expression in EPC2-ALI cells in part by STAT6-dependent mechanism.

IL-13-induced NHE3 expression and function in differentiated esophageal epithelial cells.

Employing this mature EPC2-ALI model system, we show that IL-13 stimulation of EPC2-ALI cells induced an increase in *SLC9A3* mRNA (Fig. 4A) and NHE3 protein (Fig. 4B-C) expression. Immunofluorescence analyses revealed that NHE3 was barely expressed in vehicle-treated EPC2-ALI cells (Fig. 4D, top panel). In contrast, we observed a significant increase in NHE3 expression in EPC2-ALI cells following IL-13 exposure; comparable to what we observed in EoE biopsy samples, NHE3 was predominantly localized to the basal and suprabasal layer of epithelium in IL-13-treated EPC2-ALI cultures (Fig. 4D, lower panel). To examine NHE3 function in the mature EPC2-ALI cultures, we measured proton secretion rates in an Ussing chamber system fitted with pH-STAT (Fig. 4E). We show that IL-13 stimulation reduced the extracellular pH (pH_e) compared with vehicle-treated control (pH_e 6.82 vs. 6.97, respectively, $p < 0.05$), indicating altered acid-base transport. Notably, the reduction in pH_e was abrogated with exposure to the specific NHE3 inhibitor S3226 (Fig. 4F), indicating NHE3-dependent proton extrusion. To measure the rate of acid extrusion by the mature

EPC2-ALI, the apical side buffer was adjusted to an alkaline pH [pH 7.6; Ba(OH)₂] to generate an ion concentration gradient and the amount of alkali [Ba(OH)₂] required to maintain this condition (pH 7.6) was continuously monitored using a pH-STAT (Fig. 4G). We show that IL-13 stimulation of the mature EPC2-ALI cells led to increased Ba(OH)₂ injection to counterbalance H⁺ secretion from the tissue and maintain pH 7.6 (Fig. 4G). To determine the involvement of NHE3 in apical acid secretion function in the mature EPC2-ALI, S3226 was added to the apical side of the buffer to identify the NHE3-mediated fraction of acid secretion. Notably, the acid-secretion rate in IL-13-stimulated mature EPC2-ALI cells was significantly abrogated with S3226, indicating NHE3-dependent secretion (Fig. 4H). These observations indicate an IL-13-induced increase in NHE3-dependent acid secretion in EPC2-ALI cells.

Increased SLC9A3 expression and activity is linked with DIS formation.

Given the observed association between NHE3 and acid secretion in EPC2-ALI cells and correlation between SLC9A3 expression and DIS formation in esophageal biopsy samples from patients with EoE (Fig. 4H and 1I, respectively), we examined the relationship between NHE3 function and DIS formation in the mature EPC2-ALI cells. IL-13 stimulation of EPC2-ALI cells induced DIS formation within the basal and suprabasal layer of EPC2-ALI cells as evidenced by spaces between cells (Fig. 5A). Electron microscopy analyses revealed alteration to the intercellular junctional structures of esophageal cells, with the appearance of expanded or dilated intercellular areas (Fig. 5B). Notably, the DIS are sealed by lateral membranes that are of close apposition and tethered by intercellular junctional proteins such as desmosomes (Fig. 5B). To determine the requirement of NHE3 activity in DIS formation, we stimulated EPC-ALI cells with IL-13 in the presence of the NHE3 inhibitor S3226 (Fig. 5C-D). Notably, we show that the IL-13-induced DIS within the suprabasal layer in EPC2-ALI cells were diminished in the presence of S3226 (Fig. 5C-D). Collectively, we concluded that NHE3 has an important role in IL-13-induced DIS formation in esophageal cells.

Discussion

EoE is characterized by histopathologic manifestations including BZH and DIS. The underlying molecular processes that drive these pathologic manifestations remain largely unexplored. Herein, we demonstrate 1) dysregulation of transmembrane transporter activity gene networks in esophageal biopsies from patients with EoE; 2) increased expression of the $\text{Na}^+\text{-H}^+$ exchanger *SLC9A3/NHE3* in EoE esophageal biopsies and positive correlation of this increased expression with DIS area and eosinophil infiltration; 3) increased *SLC9A3* expression and NHE3 activity in primary esophageal epithelial cells and in response to IL-13 stimulation in a mature EPC2-ALI model system; and 4) reduction of IL-13-induced DIS formation in EPC2-ALI cells by pharmacological antagonism of NHE3 activity. Collectively, we have identified a role for *SLC9A3/NHE3* in IL-13-induced DIS formation in the esophageal epithelium and provide evidence for involvement of this pathway in EoE.

The cytokine IL-13 has an important role in driving the underlying allergic inflammatory cascade and the histopathologic features of EoE²²⁻²⁴. This notion is supported by the observations that stimulating esophageal cells with IL-13 leads to a transcript signature that partially overlaps the esophageal EoE transcriptome¹⁸. Furthermore, while the primary outcome of greater than 75% decrease in peak eosinophil counts at week 12 was not met, treating patients with EoE with anti-IL-13 (QAX576) reduced intraepithelial esophageal eosinophil counts and lead to an improvement in the EoE transcriptome and clinical symptom such as dysphagia in adults with EoE²⁵. Our observation of elevated *SLC9A3* and NHE3 expression in EoE tissue samples and in both primary esophageal epithelial and EPC2-ALI cultures following IL-13 stimulation was surprising given that *SLC9A3/NHE3* expression and function is predominantly associated with induction of Th1 proinflammatory cytokines, including IFN- γ and TNF⁴⁴. IFN- γ and TNF are thought to modulate *SLC9A3* expression by PKA-mediated phosphorylation of Sp1 and Sp3 transcription factors⁴⁴. TNF has also been shown to alter NHE3 activity by stimulating PKC α -dependent internalization of NHE3⁴⁵. Stimulation of EPC2-ALI cultures with other pro-Type 2 cytokines such as IL-25 and IL-33 did not lead to induction of *SLC9A3/NHE3* mRNA expression (results not shown). Notably, a recent

study in kidney and intestinal epithelial cells (Caco-2) reported a STAT3-dependent increase in *SLC9A3* expression through the recruitment of transcriptional factor Sp1 and Sp3⁴⁶. IL-13 is known to signal through the JAK/STAT pathway, in particular through a STAT3- and STAT6-dependent signaling pathway⁴³. We reveal that STAT6 signaling plays a significant role in IL-13-induced *SLC9A3* expression in EPC2-ALI cells. Examining the *SLC9A3* promoter did not reveal the presence of STAT6 gamma-interferon-activation site (GAS) elements (results not shown), suggesting that STAT6 may indirectly modulate *SLC9A3* expression. Notably, there are recent reports of IL-13-induced, STAT6-dependent activation of EGR1 signaling pathways in EoE^{47, 48}, and previous studies in intestinal epithelial cells have revealed that overexpression of EGR1 promotes *SLC9A3*/NHE3 expression and activity⁴⁹. We are currently further pursuing the molecular basis of IL-13 transcriptional regulation of *SLC9A3* expression.

SLC9A3 as a member of the Na⁺/H⁺ exchanger family, drives Na⁺-dependent extrusion of H⁺ and is primarily involved in the regulation of [pH]_i and acid protective mechanisms⁵⁰⁻⁵³. A consequence of Na⁺-dependent acid extrusion in a multilayered stratified epithelium such as the esophageal epithelium is acidification of the intercellular spaces⁵⁴. In well-perfused tissues where there are short diffusion distances and good cell-to-capillary diffusive coupling, the acid is rapidly buffered by phosphates, proteins and HCO₃⁻⁵⁵. However, in stratified epithelium that is undergoing rapid and sustained cellular proliferation, the diffusion distances are increased leading to often-inadequate capillary perfusion, which limits the capacity of the intercellular acid-protective mechanisms and neutralization of the acidified intercellular spaces. The accumulation of acid [H⁺] in the intercellular spaces permits the formation of an electrochemical gradient and Cl⁻ diffusion, creating an osmotic force for water flux and dilation of the intercellular spaces^{56, 57}. In EoE, there is significant esophageal epithelial basal zone (BZ) expansion, and the basal cell layer can exceed 15% of the total epithelial thickness⁵⁸. We speculate that the esophageal proliferative response and the thickening of the suprabasal layer of the esophageal epithelium in EoE increases the diffusion distances, thus causing a loss in the intercellular acid-protective mechanisms and leading to DIS. Consistent with the concept of esophageal epithelial intercellular acid as a primary

driver for DIS in EoE, luminal acid has been shown to drive acidification of the intercellular spaces and DIS in non-erosive reflux disease^{55-57, 59}. Further, support for this concept, a recent study reports a strong positive correlation between BZH and DIS ($r^2 \geq 0.67$) in both proximal and distal biopsy samples from pediatric patients with EoE⁶⁰.

Interestingly, the increased esophageal intercellular acid in non-erosive reflux disease is thought to activate afferent neurons (nociceptors) within the esophageal epithelium leading to the development of heartburn^{59, 61}. Intriguingly, though not common, EoE is also associated with the development of heartburn⁴.

SLC9A3's role in the regulation of $[pH]_i$ may not simply in response to dysregulation of $[pH]_i$ but also in part fulfilling a larger role in the regulation of esophageal epithelial proliferation. Moreover, intracellular pH plays an important role in many cellular functions including proliferation⁶² and apoptosis⁶³. In tumor cells, the $[pH]_i$ is often elevated as compared to normal cells, and it is thought that the alkaline $[pH]_i$ provides an optimal environment for DNA synthesis relative to enzyme function⁶⁴. Consistent with this, growth factors such as EGF and PDGF stimulate a rapid rise in $[pH]_i$ that is a critical requirement for entry of mitogen-stimulated quiescent cells into the S phase of the cell cycle^{65, 66}. Experimental studies have identified an important role for NHE family members in the growth factor-induced increase in $[pH]_i$ and cellular proliferation^{67, 68}. The pharmacologic abrogation of mitogen-stimulated, Na^+ -dependent extrusion of H^+ and increase in $[pH]_i$ -inhibited growth factor-induced mouse bone marrow-derived macrophage DNA synthesis and prevents progression into the S phase⁶⁷. Furthermore, the rapid and transient mitogen-induced increase in NHE1 activity and $[pH]_i$ during G_2/M entry and transition is ablated in NHE1 mutant fibroblasts⁶⁸. Notably, increasing the $[pH]_i$ in the absence of NHE1 activity was sufficient to restore CDC2 activity and cyclin B1 expression and to promote G_2/M entry and transition and cellular proliferation, indicating that the NHE1-driven increase in $[pH]_i$ at the completion of S phase is an important checkpoint for progression to G_2 and mitosis⁶⁸. We speculate that IL-13 induction of *SLC9A3/NHE3* may be a critical requirement for esophageal epithelial cell proliferation via regulating $[pH]_i$. Notably, we have previously demonstrated that overexpression of IL-13 in mice leads to esophageal cell proliferation⁶⁹. Herein, we show co-localization of

NHE3 expression within the esophageal basal proliferative zone in EoE esophageal biopsy samples and IL-13–treated EPC2-ALI cultures. Furthermore, we show that stimulating EPC2-ALI cells with IL-13 induces *SLC9A3*, but not *SLC9A1*, expression and that treating mature EPC2-ALI cells with the pan NHE inhibitor ethylisopropyl amiloride (EIPA) attenuated IL-13–induced proliferation (Supplemental Figure S3). These findings support the necessity of an NHE in IL-13–induced proliferation in an esophageal epithelial model system in vitro and given the overexpression, localization and function of NHE3, we conjecture that $[pH]_i$ balance and regulation is a critical component of the observed proliferative effect that is induced by IL-13 and mediated by an NHE in esophageal epithelial cells.

Multiple compensatory mechanisms regulate $[pH]_i$ in mammalian cells and involve Na^+/H^+ exchangers, HCO_3^- transporters, lactate- H^+ transporters and vacuolar H^+ -ATPase^{70, 71}. Our gene ontology analysis supports dysregulation of these mechanisms in EoE, identifying that 5 out of the 50 individual GO nodes generated from genes significantly dysregulated in EoE are tightly correlated with the transmembrane ion transport activity. Notably, several the most dysregulated genes were part of the $[pH]_i$ regulatory circuit, including Cl^-/HCO_3^- exchangers (*SLC26A4*, *SLC4A2*, *SLC4A8*) and carbonic anhydrases (*CA2*). These functional analyses support the concept of $[pH]_i$ pathways being active in the primary esophageal epithelial cells in EoE.

The significant decrease in DIS with steroid therapy or elimination diet in patients with EoE being associated with symptom improvement³¹ indicates an association between DIS and the etiology of EoE. We demonstrate a role for *SLC9A3*/NHE3 and Na^+/H^+ exchange in DIS formation, one of the histopathologic manifestations of EoE. Given our observations, one would predict that utilizing NHE3 antagonists (systemically or topically) may be a therapeutic approach for reducing DIS and thus normalizing associated esophageal caliber dimensions in EoE. Notably, a NHE3-specific inhibitor, tenapanor, is in phase 3 clinical trials for treatment of cardiorenal and gastrointestinal disease⁷². Tenapanor has been shown to reduce sodium uptake, resulting in reduction in $[pH]_i$ ⁷². Given the contribution of DIS to esophageal barrier dysfunction and facilitating

food allergen exposure, considering potential usage of NHE3 inhibitors for EoE is warranted.

In summary, we identified a relationship between *SLC9A3*/NHE3 expression and activity with DIS in EoE. Mechanistically, we show that IL-13 stimulates *SLC9A3* expression and NHE3 activity (via $[pH]_i$) and that these were associated with esophageal epithelial DIS. Inhibiting NHE activity attenuated esophageal epithelial DIS formation, providing rationale for the therapeutic utilization of NHE3 antagonists for reducing DIS and DIS-associated esophageal pathophysiologic manifestations in EoE.

ACCEPTED MANUSCRIPT

References

1. Dellon ES, Hirano I. Epidemiology and Natural History of Eosinophilic Esophagitis. *Gastroenterology* 2017.
2. Dellon ES. Epidemiology of eosinophilic esophagitis. *Gastroenterol Clin North Am* 2014; 43:201-18.
3. Prasad GA, Alexander JA, Schleck CD, Zinsmeister AR, Smyrk TC, Elias RM, et al. Epidemiology of eosinophilic esophagitis over three decades in Olmsted County, Minnesota. *Clin Gastroenterol Hepatol* 2009; 7:1055-61.
4. Arias A, Perez-Martinez I, Tenias JM, Lucendo AJ. Systematic review with meta-analysis: the incidence and prevalence of eosinophilic oesophagitis in children and adults in population-based studies. *Aliment Pharmacol Ther* 2016; 43:3-15.
5. Liacouras CA, Furuta GT, Hirano I, Atkins D, Attwood SE, Bonis PA, et al. Eosinophilic esophagitis: updated consensus recommendations for children and adults. *J Allergy Clin Immunol* 2011; 128:3-20 e6; quiz 1-2.
6. Klinnert MD, Silveira L, Harris R, Moore W, Atkins D, Fleischer DM, et al. Health-Related Quality of Life Over Time in Children With Eosinophilic Esophagitis and Their Families. *Journal of Pediatric Gastroenterology and Nutrition* 2014; 59:308-16.
7. Akei HS, Mishra A, Blanchard C, Rothenberg ME. Epicutaneous Antigen Exposure Primes for Experimental Eosinophilic Esophagitis in Mice. *Gastroenterology* 2005; 129:985-94.
8. Collins MH. Histopathology of eosinophilic esophagitis. *Dig Dis* 2014; 32:68-73.
9. Collins MH. Histopathologic features of eosinophilic esophagitis. *Gastrointest Endosc Clin N Am* 2008; 18:59-71; viii-ix.
10. Doherty TA, Baum R, Newbury RO, Yang T, Dohil R, Aquino M, et al. Group 2 innate lymphocytes (ILC2) are enriched in active eosinophilic esophagitis. *J Allergy Clin Immunol* 2015; 136:792-4.e3.
11. Abu-Sultaneh SM, Durst P, Maynard V, Elitsur Y. Fluticasone and food allergen elimination reverse sub-epithelial fibrosis in children with eosinophilic esophagitis. *Dig Dis Sci* 2011; 56:97-102.
12. Straumann A, Conus S, Degen L, Felder S, Kummer M, Engel H, et al. Budesonide is effective in adolescent and adult patients with active eosinophilic esophagitis. *Gastroenterology* 2010; 139:1526-37, 37 e1.
13. Arora AS, Perrault J, Smyrk TC. Topical corticosteroid treatment of dysphagia due to eosinophilic esophagitis in adults. *Mayo Clin Proc* 2003; 78:830-5.
14. Faubion WA, Jr., Perrault J, Burgart LJ, Zein NN, Clawson M, Freese DK. Treatment of eosinophilic esophagitis with inhaled corticosteroids. *J Pediatr Gastroenterol Nutr* 1998; 27:90-3.
15. Kelly KJ, Lazenby AJ, Rowe PC, Yardley JH, Perman JA, Sampson HA. Eosinophilic esophagitis attributed to gastroesophageal reflux: improvement with an amino acid-based formula. *Gastroenterology* 1995; 109:1503-12.
16. Liacouras CA, Ruchelli E. Eosinophilic esophagitis. *Curr Opin Pediatr* 2004; 16:560-6.
17. Liacouras CA, Wenner WJ, Brown K, Ruchelli E. Primary eosinophilic esophagitis in children: successful treatment with oral corticosteroids. *J Pediatr Gastroenterol Nutr* 1998; 26:380-5.

18. Blanchard C, Mingler MK, Vicario M, Abonia JP, Wu YY, Lu TX, et al. IL-13 involvement in eosinophilic esophagitis: transcriptome analysis and reversibility with glucocorticoids. *J Allergy Clin Immunol* 2007; 120:1292-300.
19. Mishra A, Hogan SP, Brandt EB, Rothenberg ME. IL-5 promotes eosinophil trafficking to the esophagus. *J Immunol* 2002; 168:2464-9.
20. Mishra A, Hogan SP, Brandt EB, Rothenberg ME. An etiological role for aeroallergens and eosinophils in experimental esophagitis. *J Clin Invest* 2001; 107:83-90.
21. Mishra A, Rothenberg ME. Intratracheal IL-13 induces eosinophilic esophagitis by an IL-5, eotaxin-1, and STAT6-dependent mechanism. *Gastroenterology* 2003; 125:1419-27.
22. Blanchard C, Stucke EM, Burwinkel K, Caldwell JM, Collins MH, Ahrens A, et al. Coordinate interaction between IL-13 and epithelial differentiation cluster genes in eosinophilic esophagitis. *J Immunol* 2010; 184:4033-41.
23. Blanchard C, Stucke EM, Rodriguez-Jimenez B, Burwinkel K, Collins MH, Ahrens A, et al. A striking local esophageal cytokine expression profile in eosinophilic esophagitis. *J Allergy Clin Immunol* 2011; 127:208-17, 17 e1-7.
24. Sherrill JD, Kiran KC, Blanchard C, Stucke EM, Kemme KA, Collins MH, et al. Analysis and expansion of the eosinophilic esophagitis transcriptome by RNA sequencing. *Genes Immun* 2014; 15:361-9.
25. Rothenberg ME, Wen T, Greenberg A, Alpan O, Enav B, Hirano I, et al. Intravenous anti-IL-13 mAb QAX576 for the treatment of eosinophilic esophagitis. *J Allergy Clin Immunol* 2015; 135:500-7.
26. D'Mello RJ, Caldwell JM, Azouz NP, Wen T, Sherrill JD, Hogan SP, et al. LRRC31 is induced by IL-13 and regulates kallikrein expression and barrier function in the esophageal epithelium. *Mucosal Immunol* 2016; 9:744-56.
27. Davis BP, Stucke EM, Khorki ME, Litosh VA, Rymer JK, Rochman M, et al. Eosinophilic esophagitis-linked calpain 14 is an IL-13-induced protease that mediates esophageal epithelial barrier impairment. *JCI Insight* 2016; 1:e86355.
28. Sherrill JD, Kc K, Wu D, Djukic Z, Caldwell JM, Stucke EM, et al. Desmoglein-1 regulates esophageal epithelial barrier function and immune responses in eosinophilic esophagitis. *Mucosal Immunol* 2014; 7:718-29.
29. Purdy JK, Appelman HD, Golembeski CP, McKenna BJ. Lymphocytic esophagitis: a chronic or recurring pattern of esophagitis resembling allergic contact dermatitis. *Am J Clin Pathol* 2008; 130:508-13.
30. Caviglia R, Ribolsi M, Maggiano N, Gabbrielli AM, Emerenziani S, Guarino MP, et al. Dilated intercellular spaces of esophageal epithelium in nonerosive reflux disease patients with physiological esophageal acid exposure. *Am J Gastroenterol* 2005; 100:543-8.
31. Ravelli A, Villanacci V, Cadei M, Fuoti M, Gennati G, Salemme M. Dilated intercellular spaces in eosinophilic esophagitis. *J Pediatr Gastroenterol Nutr* 2014; 59:589-93.
32. Mueller S, Neureiter D, Aigner T, Stolte M. Comparison of histological parameters for the diagnosis of eosinophilic oesophagitis versus gastro-oesophageal reflux disease on oesophageal biopsy material. *Histopathology* 2008; 53:676-84.
33. Orłowski J, Grinstein S. Emerging roles of alkali cation/proton exchangers in organellar homeostasis. *Curr Opin Cell Biol* 2007; 19:483-92.
34. Trapnell C, Roberts A, Goff L, Pertea G, Kim D, Kelley DR, et al. Differential gene and transcript expression analysis of RNA-seq experiments with TopHat and Cufflinks. *Nat Protoc* 2012; 7:562-78.

35. Langmead B, Trapnell C, Pop M, Salzberg SL. Ultrafast and memory-efficient alignment of short DNA sequences to the human genome. *Genome Biol* 2009; 10:R25.
36. Garber M, Grabherr MG, Guttman M, Trapnell C. Computational methods for transcriptome annotation and quantification using RNA-seq. *Nature Methods* 2011; 8:469-77.
37. Kartashov AV, Barski A. BioWardrobe: an integrated platform for analysis of epigenomics and transcriptomics data. *Genome Biol* 2015; 16:158.
38. Chen J, Bardes EE, Aronow BJ, Jegga AG. ToppGene Suite for gene list enrichment analysis and candidate gene prioritization. *Nucleic Acids Res* 2009; 37:W305-11.
39. Harada H, Nakagawa H, Oyama K, Takaoka M, Andl CD, Jacobmeier B, et al. Telomerase induces immortalization of human esophageal keratinocytes without p16(INK4a) inactivation. *Molecular Cancer Research* 2003; 1:729-38.
40. Schwark JR, Jansen HW, Lang HJ, Krick W, Burckhardt G, Hropot M. S3226, a novel inhibitor of Na⁺/H⁺ exchanger subtype 3 in various cell types. *Pflugers Arch* 1998; 436:797-800.
41. Iovannisci D, Illek B, Fischer H. Function of the HVCN1 proton channel in airway epithelia and a naturally occurring mutation, M91T. *J Gen Physiol* 2010; 136:35-46.
42. Wakabayashi S, Shigekawa M, Pouyssegur J. Molecular physiology of vertebrate Na⁺/H⁺ exchangers. *Physiol Rev* 1997; 77:51-74.
43. Liu Y, Munker S, Mullenbach R, Weng HL. IL-13 Signaling in Liver Fibrogenesis. *Front Immunol* 2012; 3:116.
44. Amin MR, Malakooti J, Sandoval R, Dudeja PK, Ramaswamy K. IFN-gamma and TNF-alpha regulate human NHE3 gene expression by modulating the Sp family transcription factors in human intestinal epithelial cell line C2BBel. *Am J Physiol Cell Physiol* 2006; 291:C887-96.
45. Clayburgh DR, Musch MW, Leitges M, Fu YX, Turner JR. Coordinated epithelial NHE3 inhibition and barrier dysfunction are required for TNF-mediated diarrhea in vivo. *J Clin Invest* 2006; 116:2682-94.
46. Su HW, Wang SW, Ghishan FK, Kiela PR, Tang MJ. Cell confluency-induced Stat3 activation regulates NHE3 expression by recruiting Sp1 and Sp3 to the proximal NHE3 promoter region during epithelial dome formation. *Am J Physiol Cell Physiol* 2009; 296:C13-24.
47. Rochman M, Kartashov AV, Caldwell JM, Collins MH, Stucke EM, Kc K, et al. Neurotrophic tyrosine kinase receptor 1 is a direct transcriptional and epigenetic target of IL-13 involved in allergic inflammation. *Mucosal Immunol* 2015; 8:785-98.
48. Cho SJ, Kang MJ, Homer RJ, Kang HR, Zhang X, Lee PJ, et al. Role of early growth response-1 (Egr-1) in interleukin-13-induced inflammation and remodeling. *J Biol Chem* 2006; 281:8161-8.
49. Malakooti J, Sandoval R, Amin MR, Clark J, Dudeja PK, Ramaswamy K. Transcriptional stimulation of the human NHE3 promoter activity by PMA: PKC independence and involvement of the transcription factor EGR-1. *Biochem J* 2006; 396:327-36.
50. Brant SR, Yun CH, Donowitz M, Tse CM. Cloning, tissue distribution, and functional analysis of the human Na⁺/N⁺ exchanger isoform, NHE3. *Am J Physiol* 1995; 269:C198-206.

51. Praetorius J, Andreassen D, Jensen BL, Ainsworth MA, Friis UG, Johansen T. NHE1, NHE2, and NHE3 contribute to regulation of intracellular pH in murine duodenal epithelial cells. *Am J Physiol Gastrointest Liver Physiol* 2000; 278:G197-206.
52. Wang Z, Orlowski J, Shull GE. Primary structure and functional expression of a novel gastrointestinal isoform of the rat Na/H exchanger. *J Biol Chem* 1993; 268:11925-8.
53. Schultheis PJ, Clarke LL, Meneton P, Miller ML, Soleimani M, Gawenis LR, et al. Renal and intestinal absorptive defects in mice lacking the NHE3 Na⁺/H⁺ exchanger. *Nat Genet* 1998; 19:282-5.
54. Swietach P, Vaughan-Jones RD, Harris AL, Hulikova A. The chemistry, physiology and pathology of pH in cancer. *Philos Trans R Soc Lond B Biol Sci* 2014; 369:20130099.
55. Orlando RC. Esophageal mucosal defense mechanisms. *GI Motility online* 2006.
56. Tobey NA, Gambling TM, Vanegas XC, Carson JL, Orlando RC. Physicochemical basis for dilated intercellular spaces in non-erosive acid-damaged rabbit esophageal epithelium. *Dis Esophagus* 2008; 21:757-64.
57. Orlando LA, Orlando RC. Dilated intercellular spaces as a marker of GERD. *Curr Gastroenterol Rep* 2009; 11:190-4.
58. Noffsinger AE. Update on esophagitis: controversial and underdiagnosed causes. *Archives of pathology & laboratory medicine* 2009; 133:1087-95.
59. Barlow WJ, Orlando RC. The pathogenesis of heartburn in nonerosive reflux disease: a unifying hypothesis. *Gastroenterology* 2005; 128:771-8.
60. Collins MH, Martin LJ, Alexander ES, Boyd JT, Sheridan R, He H, et al. Newly developed and validated eosinophilic esophagitis histology scoring system and evidence that it outperforms peak eosinophil count for disease diagnosis and monitoring. *Dis Esophagus* 2017; 30:1-8.
61. Rodrigo J, Hernandez DJ, Vidal MA, Pedrosa JA. Vegetative innervation of the esophagus III. Intraepithelial endings. *Acta Anat* 1975; 92:242.
62. Pouyssegur J, Franchi A, L'Allemain G, Paris S. Cytoplasmic pH, a key determinant of growth factor-induced DNA synthesis in quiescent fibroblasts. *FEBS Lett* 1985; 190:115-9.
63. Schelling JR, Abu Jawdeh BG. Regulation of cell survival by Na⁺/H⁺ exchanger-1. *Am J Physiol Renal Physiol* 2008; 295:F625-32.
64. Moolenaar WH, Defize LH, De Laat SW. Ionic signalling by growth factor receptors. *J Exp Biol* 1986; 124:359-73.
65. Di Sario A, Svegliati Baroni G, Bendia E, Ridolfi F, Saccomanno S, Ugili L, et al. Intracellular pH regulation and Na⁺/H⁺ exchange activity in human hepatic stellate cells: effect of platelet-derived growth factor, insulin-like growth factor 1 and insulin. *J Hepatol* 2001; 34:378-85.
66. Li M, Morley P, Asem EK, Tsang BK. Epidermal growth factor elevates intracellular pH in chicken granulosa cells. *Endocrinology* 1991; 129:656-62.
67. Vairo G, Cocks BG, Cragoe EJ, Jr., Hamilton JA. Selective suppression of growth factor-induced cell cycle gene expression by Na⁺/H⁺ antiport inhibitors. *J Biol Chem* 1992; 267:19043-6.
68. Putney LK, Barber DL. Na-H exchange-dependent increase in intracellular pH times G2/M entry and transition. *J Biol Chem* 2003; 278:44645-9.

69. Zuo L, Fulkerson PC, Finkelman FD, Mingler M, Fischetti CA, Blanchard C, et al. IL-13 induces esophageal remodeling and gene expression by an eosinophil-independent, IL-13R alpha 2-inhibited pathway. *J Immunol* 2010; 185:660-9.
70. Schreiber R. Ca²⁺ signaling, intracellular pH and cell volume in cell proliferation. *J Membr Biol* 2005; 205:129-37.
71. Shrode LD, Tapper H, Grinstein S. Role of intracellular pH in proliferation, transformation, and apoptosis. *J Bioenerg Biomembr* 1997; 29:393-9.
72. Spencer AG, Labonte ED, Rosenbaum DP, Plato CF, Carreras CW, Leadbetter MR, et al. Intestinal inhibition of the Na⁺/H⁺ exchanger 3 prevents cardiorenal damage in rats and inhibits Na⁺ uptake in humans. *Sci Transl Med* 2014; 6:227ra36.

Figure Legends

Figure 1. *SLC9A3* is the most upregulated transmembrane transporter activity gene in the EoE transcriptome, and levels correlate with EoE severity and DIS. **A)** GO nodes associated with transmembrane transporter activity-related genes identified by Gene ontology (GO) enrichment analysis of 1610 dysregulated genes from RNA sequencing. **B)** Heatmap depicting the expression level of 62 individual genes within the transmembrane transporter activity GO nodes. **C)** Individual FPKM values of *SLC9A3* and **D)** Heatmap depicting expression level of *SLC9A1-9*, **E)** Correlation analysis of *SLC9A3* or *SLC9A1* expression and matched peak distal eosinophil counts/HPF in esophageal biopsies (NL = 6; EoE = 10). **F)** qPCR analysis of *SLC9A3* expression and **G)** Spearman correlation relating *SLC9A3* expression and eosinophil count/HPF in an independent validation cohort (NL = 10; EoE = 10). **H)** Immunofluorescence staining of esophageal biopsy sections from NL (top panel) and patients with EoE (lower panel). NHE3 (red), CK13 (green) and nuclei (DAPI, blue) are shown. Images are representative of 7 patients per group. Magnification x40. **I)** Spearman correlation between *SLC9A3* or *SLC9A1* expression and percentage of dilated intercellular spaces (DIS) in esophageal biopsies from patients with active EoE (n = 8). **(C, F)** Data are represented as the average \pm S.E.M. **(E, G, I)** Data are presented as relative expression over 18S. **(C, E-G, I)** Individual symbols represent an individual patient **p < 0.01, ***p < 0.001.

Figure 2. Increased *SLC9A3*/NHE3 expression and activity in primary esophageal epithelial cells derived from EoE biopsy in response to IL-13. **A)** qPCR analysis of *SLC9A3*, **B)** Baseline intercellular pH (pH_i), **C)** Representative curves of pH_i change over time and **D)** Na^+ -dependent pH_i recovery rate of cells derived from biopsies of patients with active EoE (n = 6) treated with vehicle (Veh) or IL-13. **E)** Spearman correlation analysis comparing the *SLC9A3* expression level and Na^+ -dependent pH_i recovery rate (n = 5 individual patients stimulated with vehicle and IL-13). **F)** Percentage of S3226-sensitive Na^+ -dependent intracellular recovery rate in cells treated with vehicle or IL-13. See Material and Methods for detailed protocol. **B)** Data represent the average $\text{pH}_i \pm$ S.E.M of cells from patients with active EoE (n = 8). **C)** Each data point represents the average value of 40 individual cells from 2 individual experiments. Data points for D) represent the average value of 120 individual cells from 6 different patients with active EoE and F) 50 individual cells from 5 different patients with active EoE. **(A-B, D, F)** Data are represented as the average \pm S.E.M. *p < 0.05, **p < 0.01, ****p < 0.0001.

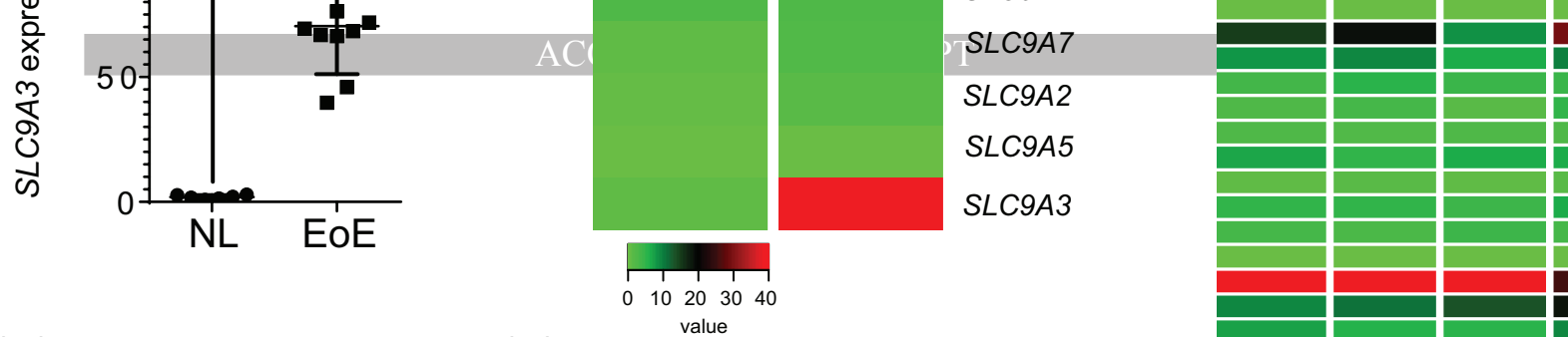
Figure 3. Mature stratified squamous esophageal epithelium model using EPC-ALI culture system. **A)** Schematic diagram of the esophageal epithelium (EPC2) air-liquid interface (ALI) (EPC2-ALI) differentiation protocol (See Material and Methods). **B)** Gene expression change of IL-13-stimulated EPC2-ALI versus non-treated EPC2-ALI compared to that of patients with active EoE versus normal control (NL) patients. Fold changes were calculated from RNA sequencing of EPC2-ALI and patient samples. Spearman correlation analysis was applied to analyze these 23660 genes. **C)** Gene ontology analysis of 572 genes that were significantly dysregulated by IL-13 treatment of EPC2-ALI cells (Fold change > 2, p < 0.05) identified 6 GO nodes related to

transmembrane transporter activity. **D)** Heatmap depicting expression level of 46 individual genes within the transmembrane transporter activity GO nodes that are significantly dysregulated in EPC2-ALI cells following IL-13 stimulation. **E)** RPKM value indicating *SLC9A3* expression level in empty control (CTRL), *STAT3* lentiviral knockdown (*STAT3KD*) and *STAT6* lentiviral knockdown (*STAT6KD*) EPC2-ALI cultures treated with vehicle (Veh) or IL-13; $n = 3$ per treatment. $**p_{adj} < 0.01$, $***p_{adj} < 0.001$.

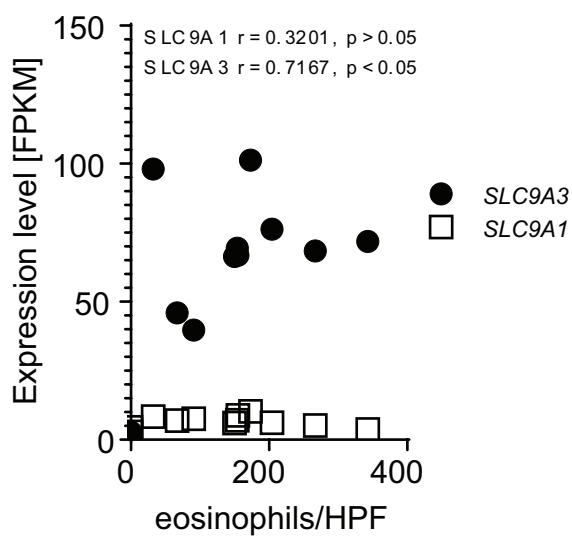
Figure 4. Increased *SLC9A3*/NHE3 expression and activity in IL-13-stimulated EPC2-ALI. **A)** qPCR, **B)** Western blot analysis and **C)** Western blot quantification of *SLC9A3*/NHE3 expression in EPC2-ALI following a 72 h-treatment with vehicle (Veh) or IL-13 (100 ng/mL). **D)** Immunofluorescence staining of vehicle (top panel) or 100 ng/mL of IL-13 (lower panel) stimulated EPC2-ALI cultures. NHE3 (red) and nuclei (blue) are shown. Images are representative of 3 samples per group. Magnification X400 **E)** Schematic view of pH-STAT assay. See Material and Methods for detailed protocol. **F)** Baseline extracellular pH (pH_e) of EPC2-ALI cells treated with vehicle or IL-13 for 72 h. DMSO (0.1%) or S3226 (30 μ M) was added to both sides of the solution during the experiment ($n = 6-11$ samples per group from 5 individual experiments). **G)** Amount of $Ba(OH)_2$ injection over time and **H)** $Ba(OH)_2$ injection rate measured for EPC2-ALI cells treated with vehicle or IL-13 (100 ng/mL) for 72 h. DMSO (0.1%) or S3226 (30 μ M) is added to both sides of the solution during experiment ($n = 6-11$ samples per group from 5 individual experiments). **(A, C, F, H)** Data are represented as the average \pm S.E.M. * $p < 0.05$; n.s. not significant

Figure 5. Blockade of NHE3 protected EPC2-ALI from IL-13-induced dilated intercellular spaces (DIS). **A)** H&E staining and **B)** electron microscopy of EPC2-ALI cultures stimulated with vehicle or IL-13 (100 ng/mL) for 72 h and showing DIS (black arrows) in only IL-13-treated cells. **C)** H&E staining of EPC2-ALI cultures stimulated with vehicle or IL-13 (100 ng/mL) in the presence and absence of S3226 (30 μ M) for 72 h. **D)** DIS formation (% of total area) was quantitated by morphometric analyses and expressed as the mean \pm S.E.M; $n = 3$ independent experiments; $****p < 0.0001$. Magnification A) X200, B) X5000 and C) X300.

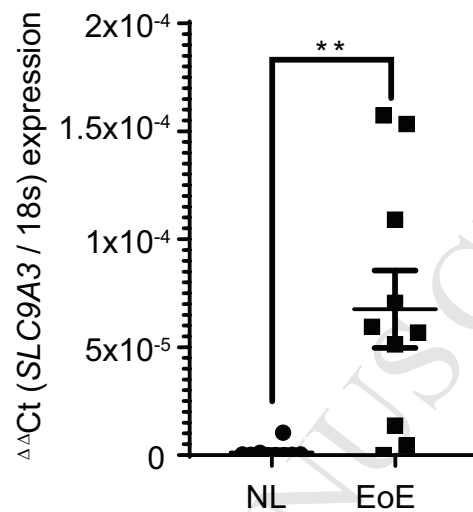
ACCEPTED MANUSCRIPT



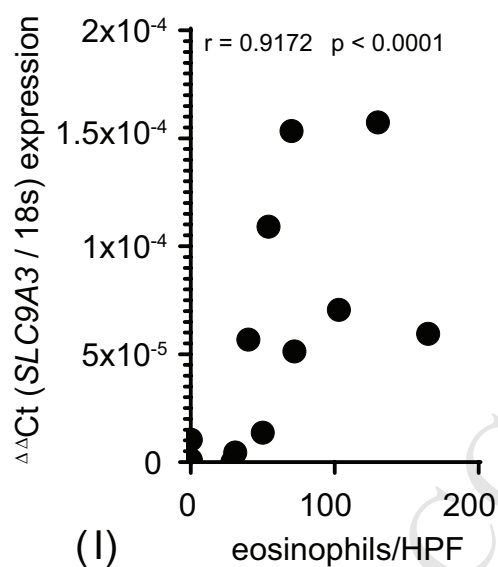
(E)



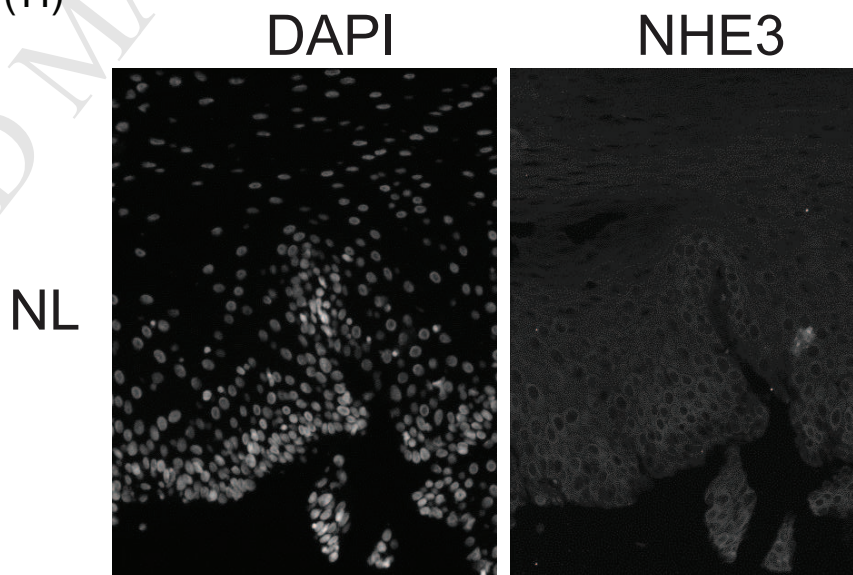
(F)



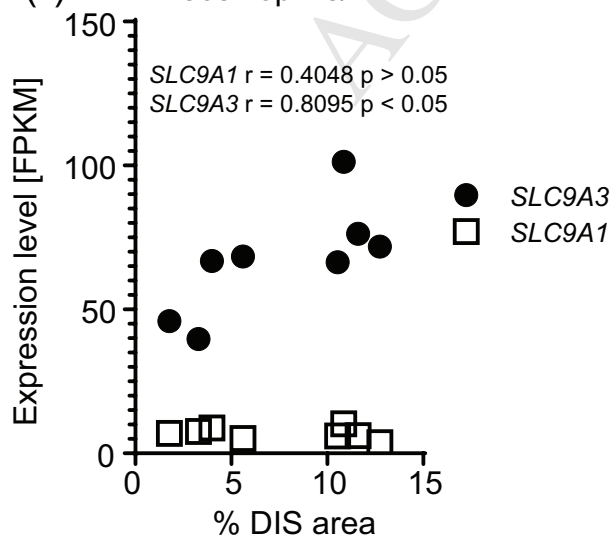
(G)



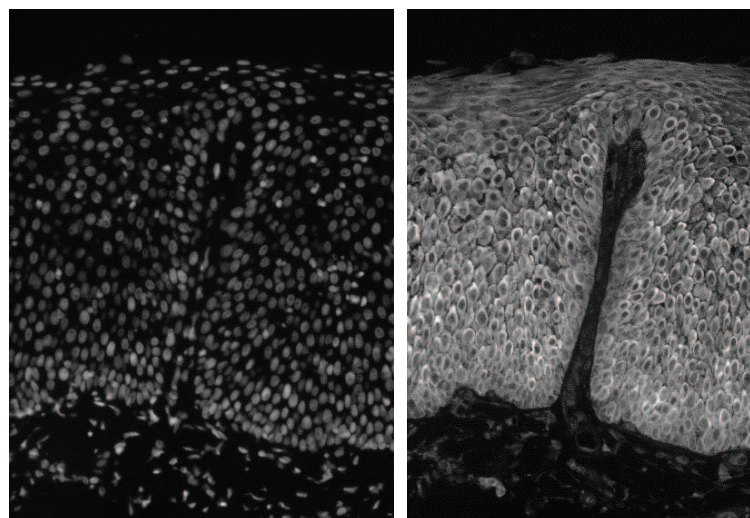
(H)

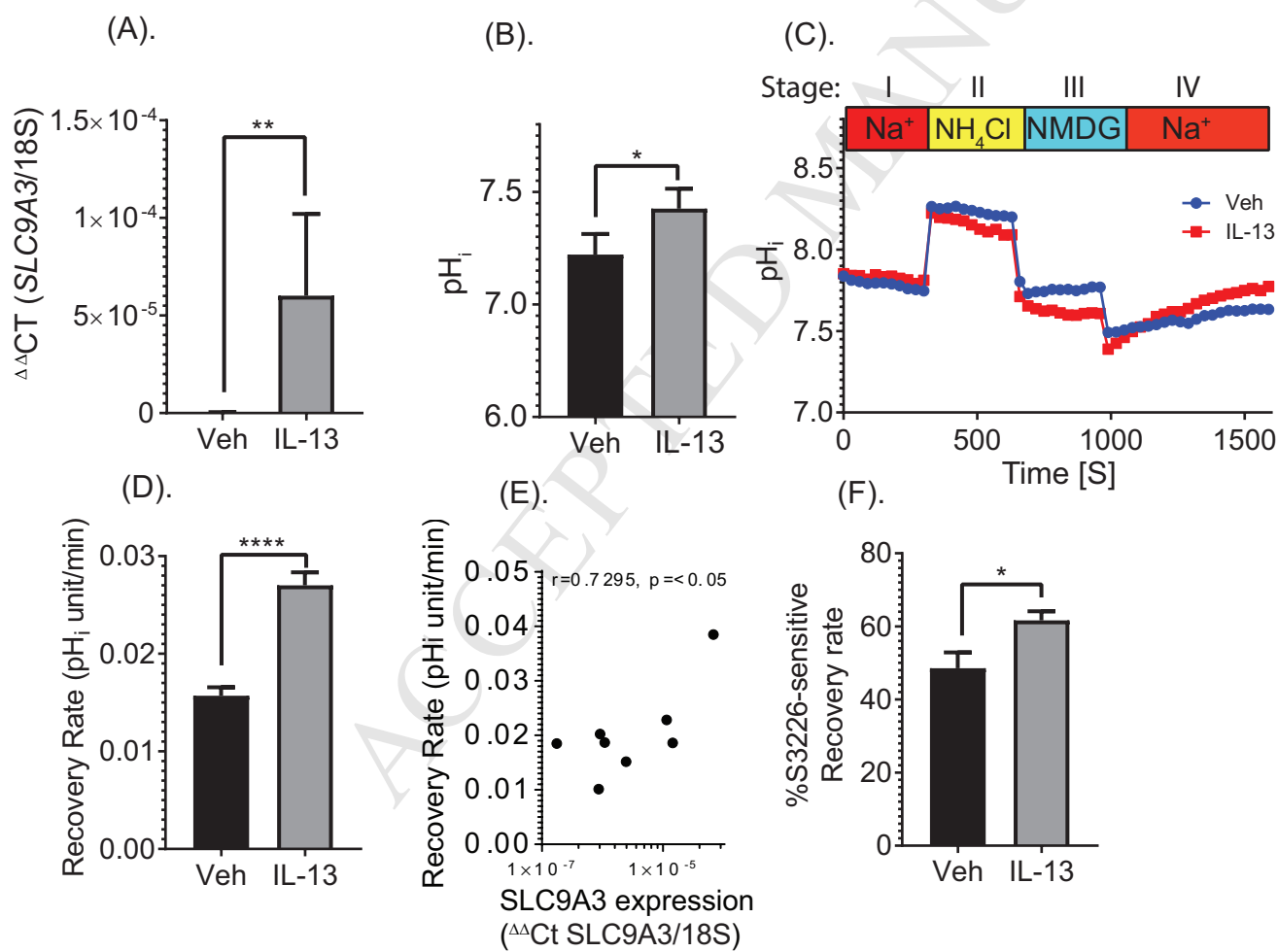


(I)



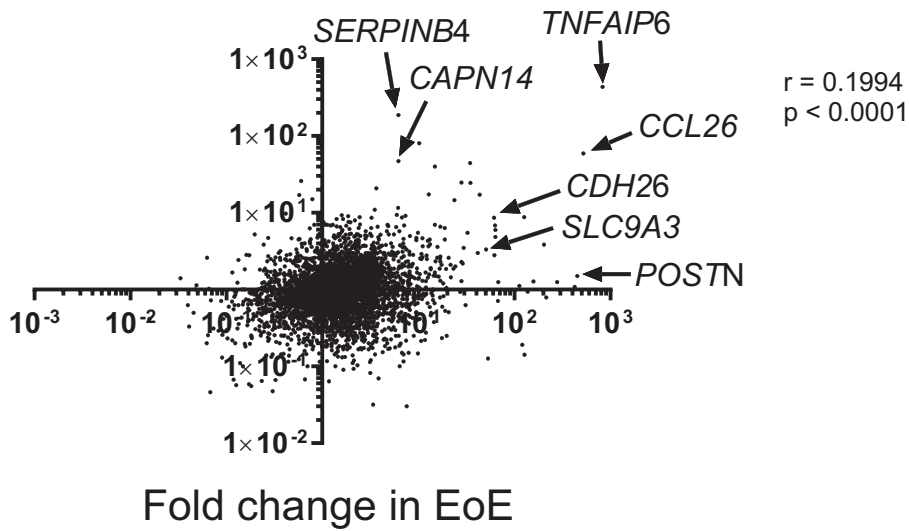
EoE





(B).

Fold change in IL13
stimulated EPC2-ALI

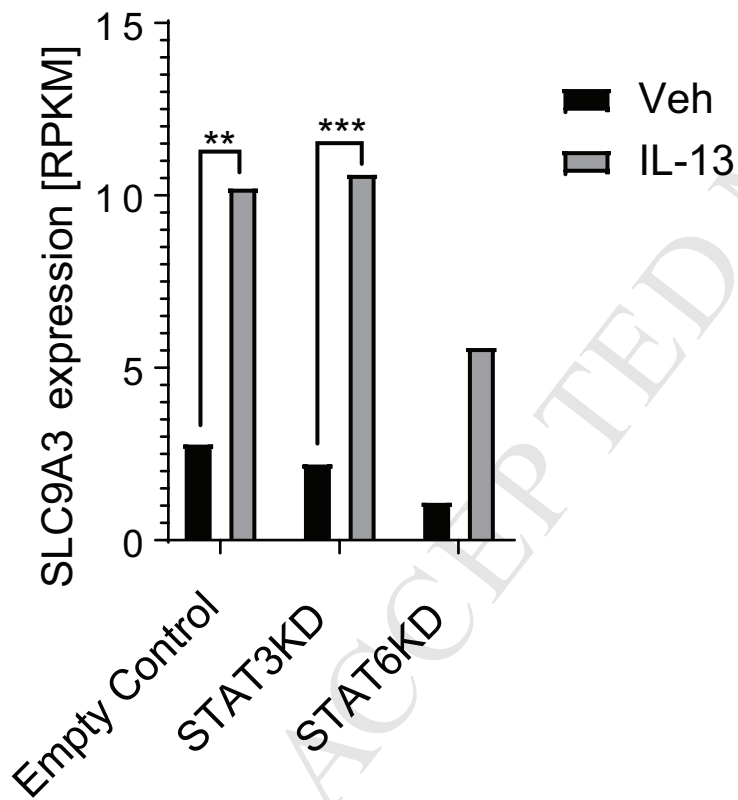


(C).

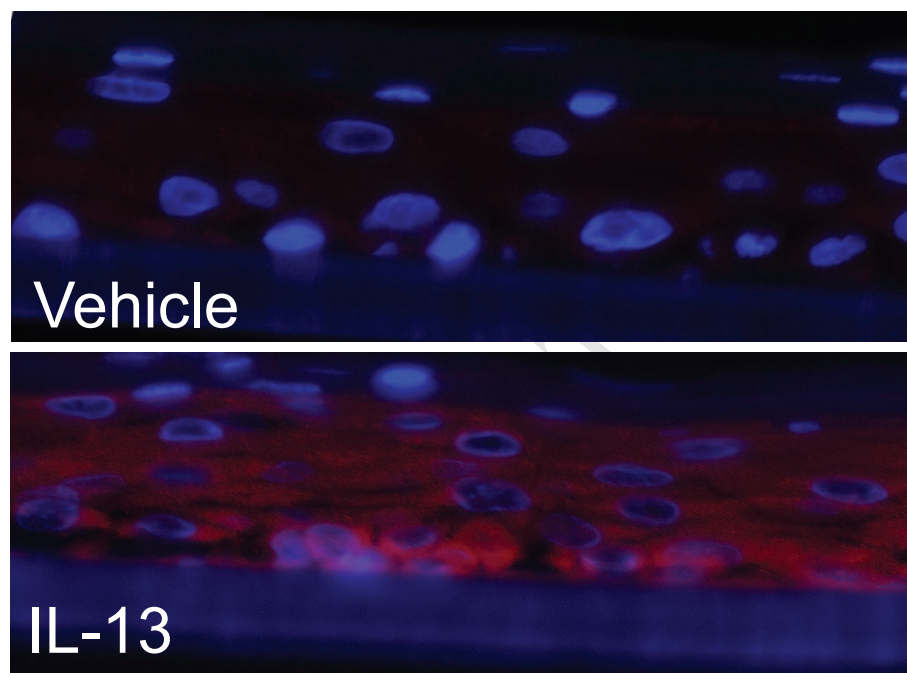
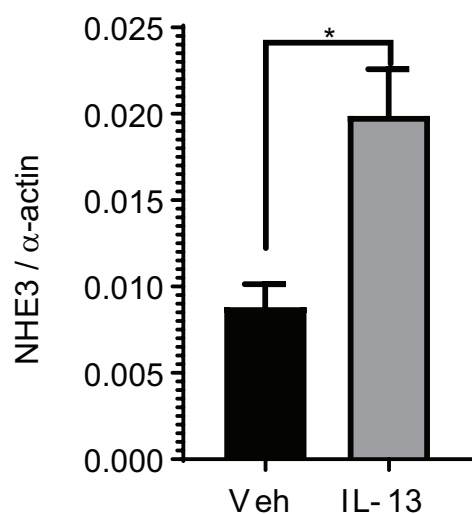
GO ID

GO:0015291	Secondary
GO:0015075	ion transmem
GO:0022891	Substrate-
GO:0022804	active transmem
GO:0008509	anion transmem
GO:0008514	organic anion

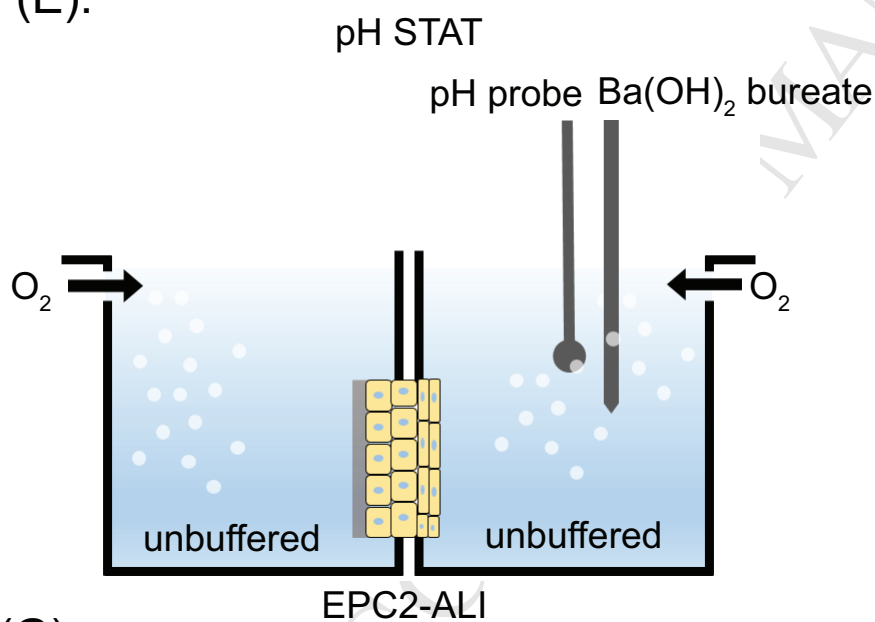
(E).



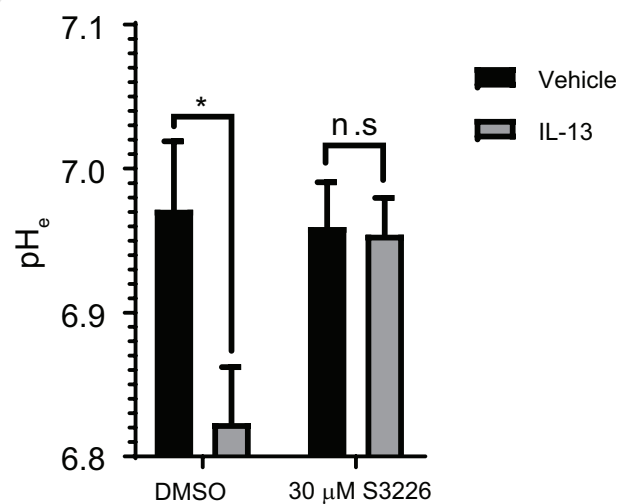
(C).



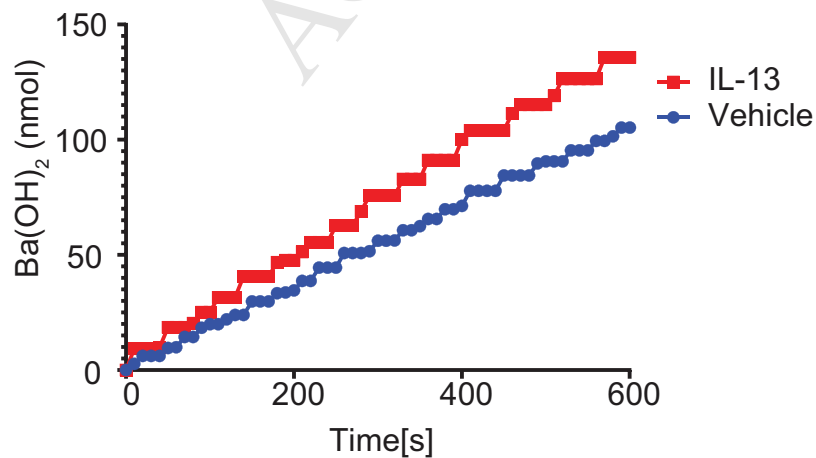
(E).



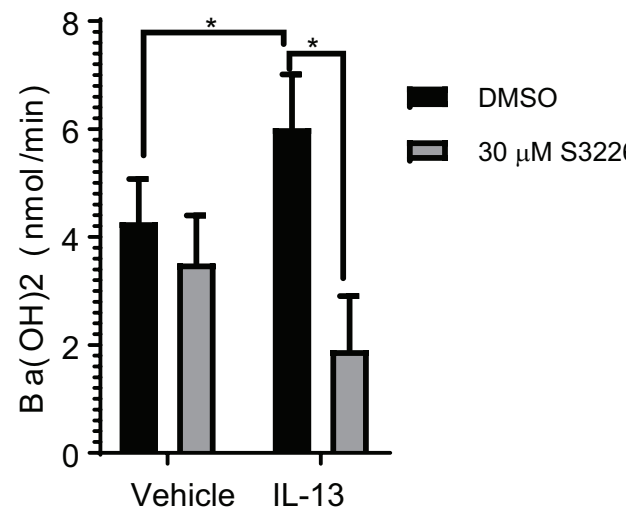
(F).



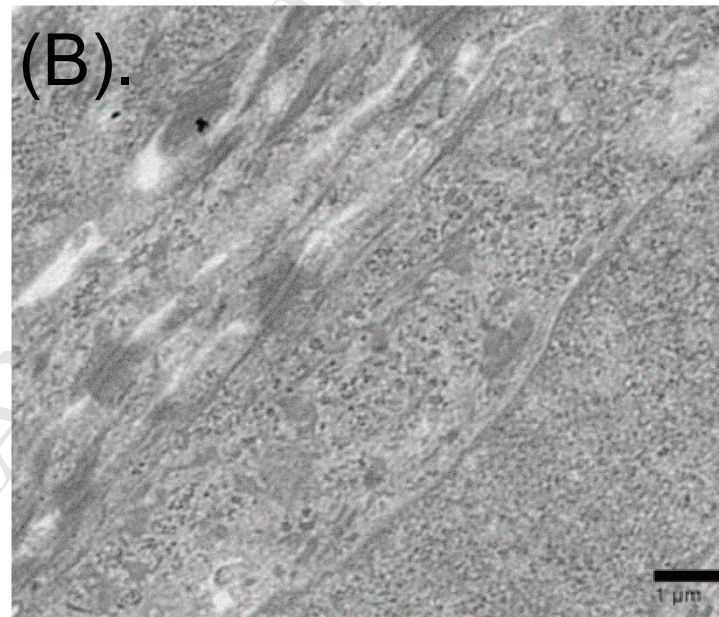
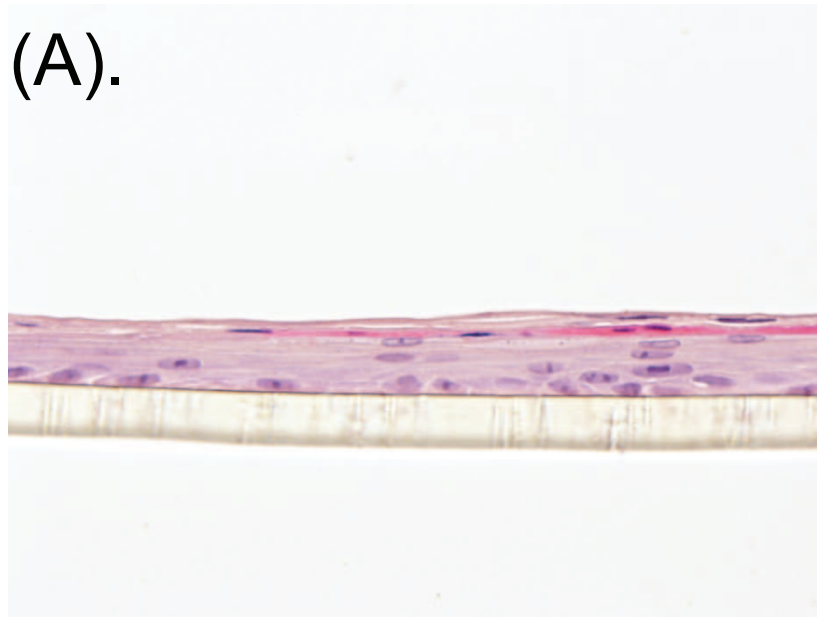
(G).



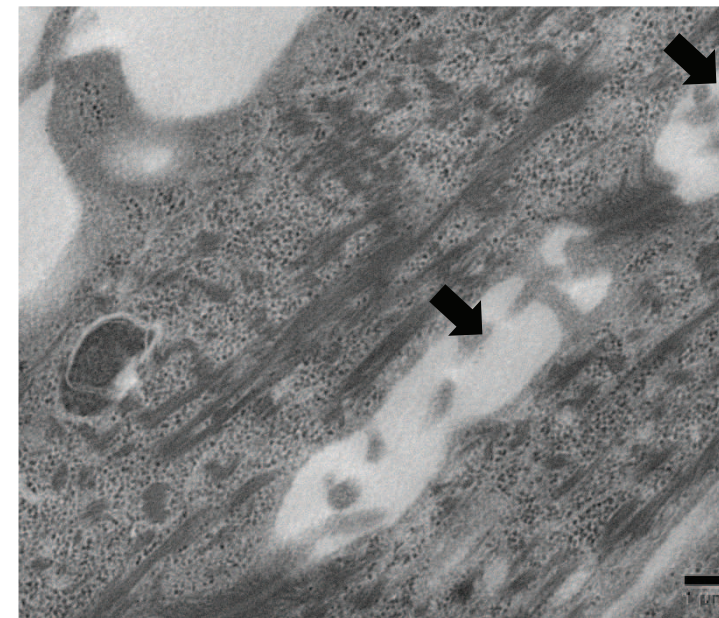
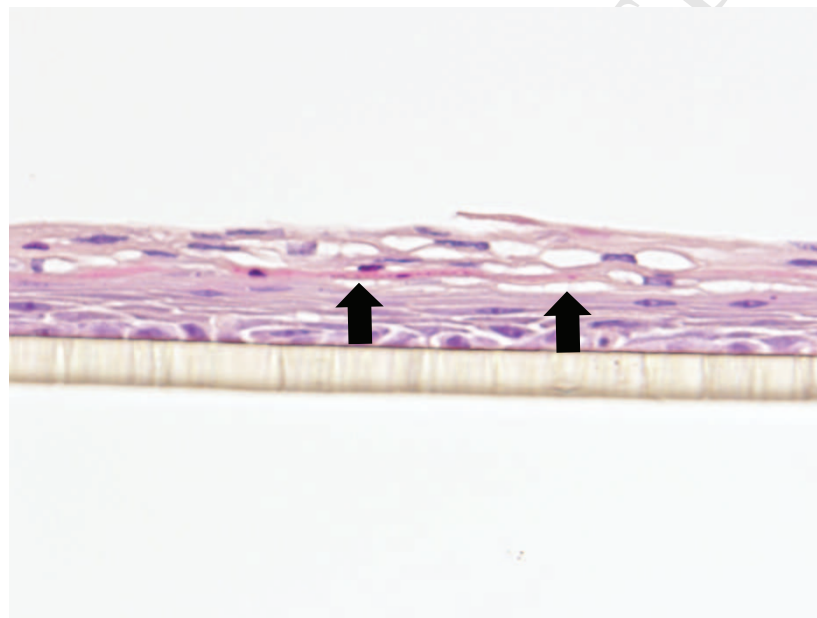
(H).



Vehicle



IL-13



Online Repository Material (Supplemental Figure Legends and Material and Methods)

Supplemental Figure 1. Patient characteristics of EoE and control patients in cohort 1 and cohort 2. Description of age of biopsy collected, gender percentage and maximum eosinophils per high power field of patient in cohort 1 (Biopsy set 1) and 2 (Biopsy set 2).

Supplemental Figure 2. The 1610 genes that were identified to be specifically dysregulated by RNA sequencing of esophageal biopsies from patients with eosinophilic esophagitis (EoE) (n = 10) and normal controls (NL) (n = 6) underwent gene ontology (GO) enrichment analysis and were clustered into 50 individual GO nodes per their molecular function (with FDR-corrected $p < 0.05$). GO enrichment based on molecular function is shown, 50 individual GO nodes are identified with FDR B&H $p < 0.05$. Blue indicates the total number of genes as part of the GO annotation; red indicates number of genes common between EoE transcriptome and GO node. Red line indicates FDR B and H p value cutoff; orange dotted line indicates FDR B and Y p value; light green dotted line indicates FDR B and H p value. Figure is generated by Toppgene.

Supplemental Figure 3. IL-13–induced proliferation in EPC2-ALI is attenuated by NHE3 inhibitor EIPA. A) EPC2-ALI cultures treated with the four combinations of vehicle (Veh) or IL-13 (100 ng/mL) with DMSO or EIPA (20 μ M) for 72 h and stained for BrdU incorporation and DAPI (nuclei). **B)** Quantification of BrdU-positive cells in EPC2-

ALI cultures. Data are presented as mean \pm SEM; n = 6 per treatment. ****p < 0.0001.

Magnification X300.

Supplemental Table 1. Expression level of 572 genes dysregulated in mature EPC2-ALI by IL-13. RPKM value of gene expression level in mature EPC2-ALI treated with vehicle (Veh) or IL-13 (100 ng/mL) for 48 h. Log₂ fold change (LOGFC) indicates the gene expression fold change induced by IL-13. n = 3 per treatment; 572 genes were selected with |LOGFC| > 1 and p < 0.05.

Supplemental Table 2. GO analysis of IL-13-induced dysregulated genes in mature EPC2-ALI. GO enrichment based on molecular function, biological pathway and pathway are shown. The p value was calculated on the basis of probability density function.

Supplemental Figure Methods:

BrdU assay. After EPC2-ALI cultures were treated as indicated in the experiment, BrdU reagents dissolved in DMSO (final concentration 10 μ M) were added to both the upper and lower chambers of transwells for 2 h. EPC2-ALI cultures were then washed with PBS and fixed with 4% paraformaldehyde for another 2 h.

Supplemental Table S1

gene_id	48h Veh	48h IL-13	LOGFC	P value
NTRK1	0	12.8962	12.0048	7.72E-25
ATP5J2-PTCD1	0	2.89614	10.92178	4.59E-15
TREML2	0	1.59001	9.500339	1.66E-07
FGF19	0	2.40941	9.285919	9.07E-07
DYX1C1-CCPG1	0	0.996634	9.175073	2.04E-06
PPT2-EGFL8	0	1.44493	8.900974	1.26E-05
TNFAIP6	0.417235	183.29	8.662212	2.90E-45
ARPC4-TTLL3	0	0.708783	8.407443	0.000188
ZNF20	0	0.923428	8.407443	0.000188
CSF3	0	1.32101	7.949604	0.001337
SHC4	0	0.446474	7.949604	0.001337
C17orf61- PLSCR3	0	0.896016	7.757792	0.002667
FAM26D	0	1.11879	7.65139	0.003799
C8orf44-SGK3	0	0.348911	7.595093	0.004545
NELL2	0	0.479493	7.475448	0.006542
SERPINB4	1.15211	214.884	7.426299	6.27E-40
SLC5A5	0	0.337742	7.201519	0.013904
MAOB	0	0.391933	6.955428	0.025126
CCDC103	0	0.597608	6.863093	0.030786
LRRC31	0	0.386815	6.863093	0.030786
CADM2	0	0.10635	6.764443	0.037847
CCL26	0.37199	21.8657	6.751451	7.30E-11
ALOX15	0	0.307886	6.658548	0.046698
TMEM191A	0	0.422046	6.658548	0.046698
FAM26E	0.111923	8.87311	6.192024	1.08E-19
ANO1	0.233214	10.1932	5.662446	8.53E-23
CAPN14	11.5813	546.537	5.443614	5.67E-15
LBH	0.337045	13.5442	5.211747	1.96E-19
DPP4	0.964848	23.7153	4.502532	9.19E-22
BCL2L15	0.0199123	0.48573	4.491584	0.002442
FCGBP	0.0120834	0.259852	4.309746	0.000157
OSR1	0.104566	2.08085	4.197853	0.000294
C1QTNF1	0.457086	7.90129	4.14251	9.17E-12
SOCS1	0.488605	8.46859	3.998544	3.81E-07
EML5	0.0828536	1.35625	3.916082	8.80E-07
SLCO2A1	0.0937948	1.35472	3.735509	8.01E-05
GLDC	0.0519947	0.734296	3.703088	0.003112
NFE2	0.17579	1.58641	3.601208	0.004677
LMO2	0.1237	0.836398	3.565584	0.04179
TMEM176A	0.0953987	1.16355	3.491584	0.049478

PSMC3IP	0.257843	1.37932	3.197853	0.018798
CDH26	2.91177	25.124	3.134618	4.55E-13
CISH	4.78419	44.7131	3.125573	2.49E-13
EDNRA	0.400461	3.44915	3.098317	1.49E-06
TMPRSS2	0.184351	1.71595	3.084959	0.000545
S100A7A	0.0694255	0.638786	3.084959	0.008248
ATP13A5	0.108312	0.973403	3.051011	0.003533
EDAR	0.140993	1.22186	2.998544	0.000899
ROR1	0.0496481	0.490605	2.944096	0.038502
KRT27	0.184288	1.49847	2.906621	0.015563
KAL1	0.0940993	0.745001	2.868147	0.00182
C16orf59	0.182476	1.36661	2.787977	0.02287
PDE6A	0.0526536	0.371801	2.703088	0.02961
TNC	16.9492	119.52	2.701126	3.33E-07
LYPD6B	2.51809	17.6597	2.693218	7.44E-08
CYP1B1	3.28606	22.9077	2.684562	7.77E-11
FAM115C	0.222967	1.49912	2.663195	0.000713
SUSD2	0.404433	2.73598	2.641249	0.000245
NBL1	2.58312	17.0047	2.63068	2.78E-08
FETUB	4.44299	29.8103	2.629371	3.67E-09
UGT2B17	0.143098	0.918593	2.565584	0.043728
SECTM1	1.82253	11.5601	2.548306	3.63E-07
IL32	0.438112	2.78624	2.529059	0.025765
LURAP1L	5.66902	34.0519	2.469724	2.17E-09
RASGRP1	1.29847	7.50046	2.45311	9.42E-08
PRICKLE4	1.92513	11.1222	2.413581	1.09E-05
MB	0.874594	4.3936	2.395659	0.004687
MKX	0.27223	1.55531	2.38116	0.003579
GLI1	0.125642	0.631713	2.372939	0.041457
UNC93A	0.281245	1.32395	2.347993	0.027743
ST6GAL1	2.75556	14.4354	2.287356	4.93E-08
ANKRD33B	0.604775	3.16028	2.268747	1.91E-06
RNF122	0.424085	2.2119	2.266024	0.01191
TGM3	5.88151	30.6317	2.263929	3.70E-08
IL2RG	0.322764	1.65754	2.243656	0.038637
SERPINB3	177.206	904.027	2.234098	0.000169
ABLIM2	0.583637	2.64277	2.209441	0.001872
GPC6	0.292805	1.44999	2.191189	0.000726
NPNT	0.438648	2.14552	2.188515	0.000906
SLC7A4	0.256871	1.26419	2.182256	0.032189
SLC26A2	2.39129	11.1783	2.108001	2.06E-07
LOC645638	23.5999	110.244	2.107006	3.56E-07

PPYR1	0.405006	1.8849	2.101637	0.022824
CTSC	86.6005	389.937	2.090948	5.58E-05
DNER	0.423696	1.92332	2.065658	0.006451
HECW2	0.157272	0.67917	1.993678	0.01682
LINC00476	0.562423	2.07078	1.959863	0.048518
MAP3K14	2.10046	8.56304	1.920289	1.37E-05
AKAP2	3.79869	15.4173	1.90406	1.94E-06
CHI3L2	1.64993	6.31169	1.900004	0.003662
LOX	0.400767	1.55909	1.899008	0.005648
GCNT3	19.0739	76.0969	1.8794	2.98E-06
PTCHD4	1.25931	4.84785	1.85371	0.000866
HS3ST1	3.88032	14.8807	1.82236	7.76E-05
DPYD	1.37435	4.88437	1.815443	0.00029
PRR9	3.30348	12.4651	1.798994	0.001009
SEMA3A	0.22748	0.853696	1.791144	0.026732
NMI	3.21376	12.0343	1.787977	0.000618
ALDH9A1	18.1412	67.8892	1.787077	8.53E-06
LAMP3	1.24484	4.60435	1.770202	0.00116
CFB	0.678504	2.49234	1.760232	0.015186
PDCD1LG2	0.73715	2.70776	1.760232	0.015186
TGM2	1.99162	7.11691	1.751657	0.000158
DIO2	2.24815	8.1191	1.724783	3.73E-05
SFRP1	7.29323	25.9703	1.715393	1.57E-05
SLC16A14	0.382766	1.34418	1.695352	0.023025
RPTN	130.765	456.312	1.686209	0.005013
ZNF860	0.432419	1.48748	1.66512	0.037828
C1S	0.619963	1.97069	1.653047	0.03097
SLC9A3	3.1023	10.3236	1.617697	0.000391
PKD2	4.13331	13.1789	1.556026	0.000116
CLGN	0.831392	2.55356	1.552409	0.025808
SCLY	1.12276	3.49355	1.544826	0.016068
ADAM8	3.94848	12.3019	1.529059	0.000355
PPP1R3C	2.694	8.4245	1.528001	0.001579
SLC45A4	3.43181	10.5442	1.502575	0.00055
ID3	22.8578	69.6206	1.48999	0.000173
PHF17	1.05748	3.16967	1.48615	0.004017
PAPSS2	0.927162	2.72897	1.471925	0.014292
CDC45	1.45115	4.32246	1.466049	0.025636
EHD3	5.62808	16.7135	1.453461	0.000308
CDC6	0.746004	2.20703	1.448015	0.037464
MUTED-TXNDC5	2.10105	6.20834	1.447056	0.002885
PPP1R3D	12.3208	36.1941	1.438288	0.000267

SLC16A9	0.620917	1.78567	1.407155	0.038559
NUDT3	1.61044	4.5133	1.396608	0.01802
BTBD3	6.46411	18.8548	1.395777	0.000416
SDSL	1.84296	5.18726	1.376107	0.041176
PGBD5	1.62383	4.56755	1.375186	0.008955
MME	9.26011	25.6182	1.355959	0.000607
ST8SIA1	0.417951	1.15826	1.35371	0.019406
TNFRSF19	0.992628	2.7798	1.345536	0.020287
TRIM16L	3.04766	8.33872	1.335287	0.009187
PDZK1IP1	30.0173	81.8403	1.330179	0.000825
NCF1	4.03745	11.0037	1.32963	0.011062
MAOA	11.7049	31.5023	1.311863	0.000988
PPARGC1B	1.25664	3.36902	1.309424	0.002308
CA2	345.751	919.198	1.293803	0.03045
IRF1	2.47978	6.4926	1.271749	0.006422
BARD1	1.48879	3.89634	1.271137	0.032774
PP7080	8.46504	21.9548	1.258108	0.002991
CALCRL	0.753184	1.9467	1.253117	0.037427
NNMT	4.89472	12.5683	1.243656	0.010111
CAT	22.1727	56.8231	1.240852	0.001614
EEF1E1-MUTED	2.22758	5.6761	1.238263	0.01409
LTA4H	75.9864	193.943	1.235562	0.00523
ITPRIPL2	5.03939	12.7608	1.217592	0.001929
CANT1	23.4506	59.2563	1.214236	0.002587
SAA1	15.5576	39.0059	1.212913	0.011045
FAM217B	7.83605	19.6528	1.21259	0.001995
SGK1	24.1875	60.2575	1.20568	0.002264
DDX58	1.31171	3.27457	1.203014	0.019629
PIK3R3	1.39546	3.36954	1.196038	0.014162
MSRB1	7.53364	18.6003	1.187073	0.008886
ORAI1	7.44987	18.2405	1.175021	0.008484
CDCA5	1.61452	3.94824	1.173267	0.046253
NINJ1	12.9094	31.4112	1.166014	0.005354
SPSB1	5.59134	13.6025	1.165768	0.005048
ENTPD2	5.09431	12.1684	1.161602	0.010615
NPDC1	3.36992	8.11224	1.150547	0.036634
GPRIN2	4.34553	10.391	1.140897	0.018744
BIRC3	0.931928	2.36181	1.122155	0.02956
PARP12	3.29122	7.76348	1.121245	0.010631
CD14	5.92275	13.752	1.119566	0.01736
DUOX2	1.93491	4.53761	1.112827	0.011514
GJA9-MYCBP	2.64351	6.47864	1.111019	0.025506

MFHAS1	2.92078	6.82238	1.107083	0.009092
RUNX2	1.15696	2.67917	1.106153	0.031511
ASB1	6.79675	15.787	1.098983	0.004983
NANOS1	2.05453	4.57482	1.038072	0.026567
LRP12	6.96458	15.3995	1.035181	0.009178
TMTC3	6.61259	14.676	1.033336	0.008207
RAB27A	3.6526	8.01938	1.027928	0.01993
VWF	2.3094	5.08792	1.022722	0.012611
ALOX15B	6.9515	14.6907	1.021935	0.014344
CST3	193.576	423.969	1.014224	0.01734
TXN	124.236	269.499	1.001292	0.014368
SLC22A23	33.8029	18.2844	-1.0035	0.013808
ID1	69.9144	37.4873	-1.00924	0.010038
WNT7A	15.2522	8.19617	-1.01284	0.020001
TNS1	1.35874	0.72994	-1.01325	0.044735
ANXA9	50.8149	27.2877	-1.01384	0.009358
ITGB6	15.0787	8.08837	-1.01543	0.014282
NLRX1	22.6021	12.1086	-1.01668	0.009196
WWC1	12.1696	6.52788	-1.01798	0.009139
C6orf15	56.5726	30.2725	-1.01893	0.009637
LDLR	93.8748	49.8872	-1.01944	0.026684
PLEKHA6	1.74968	0.934552	-1.02158	0.047762
CLIC3	132.641	70.8381	-1.02176	0.008955
GBA	35.577	18.5995	-1.022	0.008824
MANSC1	18.9684	10.1286	-1.022	0.011745
POF1B	67.1948	35.7603	-1.02683	0.014242
S100A10	407.64	216.368	-1.03065	0.022404
PPP1R12B	3.05278	1.72252	-1.03402	0.015542
PIM1	77.64	41.1106	-1.03412	0.011265
KLK13	18.4194	9.75228	-1.03425	0.020384
AKR1C2	9.38037	5.25946	-1.0344	0.018703
RNF222	6.36259	3.35871	-1.03855	0.024965
CTGF	6.55088	3.44557	-1.04378	0.034145
LCE3E	493.985	259.781	-1.04401	0.014283
LPIN1	19.0839	9.85132	-1.0449	0.007464
PPARD	43.0156	22.4969	-1.04655	0.008629
IRS1	10.6324	5.581	-1.0467	0.007332
KIAA1239	1.58926	0.833159	-1.04852	0.048315
TP53INP2	36.9779	19.3598	-1.05044	0.008195
ARHGEF4	72.9352	38.0041	-1.05271	0.012202
WNT10A	8.63071	4.49651	-1.05751	0.021095
TUFT1	24.4823	12.7784	-1.05765	0.006907

NFASC	3.93257	2.17929	-1.0605	0.045469
LRP1	10.7551	5.58044	-1.0634	0.007641
GRB7	26.5239	13.6355	-1.06389	0.007208
AIM1L	28.2062	14.6282	-1.0641	0.007288
TIMP3	6.37175	3.30232	-1.06505	0.010695
TCP11L2	16.251	8.39722	-1.06938	0.010085
SPIN4	5.27389	2.72075	-1.0717	0.018055
C9orf169	56.4704	29.1204	-1.0723	0.00863
TPRG1	8.4483	4.33235	-1.07711	0.011312
SYT8	58.2452	29.7508	-1.08605	0.005476
WFDC5	102.818	52.3894	-1.08958	0.005332
UGCG	29.0211	14.7322	-1.09497	0.006647
ARID5B	8.17082	3.89986	-1.10212	0.00538
SRPX2	6.14943	3.10577	-1.10234	0.031874
DUSP1	28.67	14.4784	-1.10248	0.005485
IGFBP3	4.24878	2.15771	-1.10427	0.042708
NCCRP1	96.0627	48.3596	-1.10701	0.006143
KAT2B	20.1373	10.0805	-1.11514	0.004334
CPA4	21.3155	10.6498	-1.11755	0.00481
PLEKHM1P	5.35447	2.6758	-1.11761	0.023359
KRT2	5.53779	2.76491	-1.11891	0.029953
SLC39A2	15.204	7.5445	-1.11891	0.01414
SERPINB1	67.5999	33.7513	-1.11891	0.004216
PLK3	28.2309	14.0973	-1.12076	0.004459
MYOM1	1.74526	0.868805	-1.12744	0.048521
GLRX	33.8623	17.0859	-1.12831	0.006211
AADACL2	7.19573	3.55973	-1.13221	0.03983
CCDC88B	3.32092	1.64085	-1.13398	0.02007
RORA	3.55452	1.75489	-1.1341	0.006191
KLK5	118.993	58.9909	-1.13451	0.00456
CAMK2N1	31.8426	15.7092	-1.13619	0.003789
HS3ST6	15.2918	7.54181	-1.13662	0.020009
HMOX1	53.996	26.626	-1.13685	0.003664
KIFC3	25.733	12.6092	-1.14554	0.003418
KIAA1199	3.66444	1.79567	-1.14591	0.009087
MYLK	2.73077	1.06278	-1.14919	0.017331
OTUB2	3.42608	1.6741	-1.15001	0.026372
ASPRV1	27.1928	13.2455	-1.15456	0.003652
SLC37A2	57.6277	28.055	-1.15551	0.005243
OSBP2	6.79934	3.29551	-1.16173	0.006903
SH3D21	4.31603	2.08801	-1.16198	0.039352
PADI3	3.88268	1.8743	-1.16754	0.027452

FBXO32	4.16856	2.02648	-1.16969	0.006959
IFITM1	20.4401	9.84087	-1.17138	0.020119
TRIB2	5.63118	2.47007	-1.17138	0.00959
LRRC20	26.212	12.6197	-1.17196	0.002779
LGALS1	60.4183	28.9347	-1.17902	0.004201
MAP3K9	7.74508	3.68914	-1.18683	0.003677
INHBA	11.2455	5.34837	-1.18901	0.007588
GDPD3	26.4244	12.5628	-1.18955	0.005881
GLTP	345.911	163.935	-1.19411	0.021022
IMPA2	60.4967	28.6608	-1.19461	0.002277
TNFAIP8L3	10.3497	4.89841	-1.19604	0.007817
PADI1	26.8216	12.6902	-1.19652	0.002251
CALML5	116.432	54.9315	-1.20062	0.002173
DUSP16	27.5642	12.9913	-1.20209	0.002739
SLC6A6	2.30587	1.27922	-1.2038	0.016779
SCNN1B	26.2716	12.2874	-1.21316	0.002117
PTPRH	2.52051	1.18113	-1.21578	0.033522
SRPX	4.87309	2.2492	-1.21578	0.040778
SASH1	17.2383	8.03138	-1.21873	0.002016
FOSL1	13.5356	6.28807	-1.22291	0.007033
DUSP6	46.8348	21.7271	-1.22541	0.0019
GJB4	4.39331	2.03682	-1.22583	0.020898
PCSK5	3.59228	1.37804	-1.22697	0.009194
SPARC	35.0307	16.1307	-1.23565	0.001705
NFATC2	2.56734	1.15494	-1.23715	0.009305
KRT79	5.7037	2.61528	-1.24177	0.021659
TMPRSS13	19.267	9.35643	-1.24444	0.001936
SH3TC2	0.648238	0.296549	-1.24509	0.010234
LIPN	18.1171	8.28438	-1.24573	0.006581
TINAGL1	50.7916	23.1182	-1.25105	0.001422
UCA1	5.30638	2.4174	-1.25111	0.019222
KRT78	223.834	101.964	-1.25121	0.004783
NDRG1	447.095	203.287	-1.25432	0.03493
LIPG	8.05869	3.65343	-1.25813	0.003009
FLG2	90.5457	41.0166	-1.25928	0.01509
C10orf116	70.1305	31.7259	-1.26011	0.001932
MALL	21.6099	9.78108	-1.26046	0.001456
TNFSF9	8.20738	3.70328	-1.26496	0.014626
LYNX1	1381.19	620.621	-1.26535	0.014294
MBOAT2	38.2663	17.2118	-1.26952	0.001376
SPRR2G	1148.07	515.868	-1.27097	0.011861
IL6R	8.33919	3.67472	-1.27134	0.001737

MATN2	2.96072	1.33777	-1.28289	0.017476
PNPLA1	3.27661	1.49227	-1.28884	0.035963
SLURP1	306.661	135.656	-1.29352	0.001219
KIF13B	16.4814	7.27326	-1.297	0.001078
IL18	43.2525	19.0087	-1.30428	0.001285
S100A12	164.048	72.024	-1.30441	0.000931
ADSSL1	6.82477	2.959	-1.30568	0.016037
HSPA2	8.0106	3.51235	-1.30631	0.00434
H19	153.395	67.2493	-1.30681	0.002661
GLUL	195.441	86.4826	-1.3122	0.011754
EEPD1	1.58455	0.691679	-1.31274	0.03769
GABRE	14.8599	6.4333	-1.32463	0.001158
CRCT1	846.618	364.754	-1.33163	0.005276
RASAL1	2.18686	0.96451	-1.33254	0.030061
PEG10	5.88086	2.51982	-1.34131	0.001307
SPON2	6.26296	2.67543	-1.34131	0.014396
IL22RA1	13.2388	5.62271	-1.35228	0.001173
ARHGAP29	9.01501	3.82781	-1.35265	0.000591
FGFBP1	243.257	102.98	-1.35696	0.001617
TRPV3	3.71045	1.56017	-1.36041	0.002965
GLA	26.3971	11.1174	-1.36439	0.001144
GNAO1	1.86537	0.805934	-1.3664	0.013094
FAM49A	2.44451	1.02811	-1.3664	0.013094
B4GALNT3	27.6506	11.5929	-1.37091	0.000487
DNAJB5	8.80537	3.71198	-1.37432	0.0029
SPNS2	70.9613	29.6095	-1.37812	0.001225
PNLIPRP3	75.8125	31.6181	-1.37852	0.000605
DSG1	75.8771	31.5732	-1.3818	0.001931
SMAD3	19.8634	8.22074	-1.38942	0.000429
CDSN	85.951	35.5609	-1.39006	0.000703
PRSS22	16.7898	6.92537	-1.39446	0.002221
GRAMD1C	6.75636	2.82685	-1.39575	0.002047
CLCA4	28.7374	11.7299	-1.4042	0.000359
RUSC2	7.6773	3.09819	-1.4065	0.000671
IL37	8.52204	3.3792	-1.4117	0.036442
ARRB1	0.765803	0.313581	-1.41931	0.041956
BHLHE41	1.41463	0.571764	-1.42377	0.045085
SLC15A1	7.34683	2.96794	-1.4245	0.001871
THEM5	13.0476	5.26949	-1.42489	0.005312
MUC20	3.88438	1.56977	-1.42728	0.001667
SLC16A5	6.22436	2.50965	-1.42728	0.00898
CRLF1	2.79946	1.12757	-1.42877	0.048549

CDA	24.7818	9.87636	-1.44407	0.001515
OVOL2	5.79497	2.28922	-1.45678	0.015159
CSGALNACT1	3.14939	1.32582	-1.46089	0.006164
NOS3	1.46849	0.581862	-1.47094	0.029232
SPTSSB	16.5755	6.47796	-1.47228	0.000464
FOS	6.79126	2.65107	-1.47394	0.004294
FHDC1	7.86995	3.07043	-1.47475	0.00029
C1QTNF6	5.80248	2.26082	-1.48217	0.002758
MYCT1	3.02636	1.16981	-1.48815	0.012706
KLK9	16.5958	6.40971	-1.48932	0.001097
FAM43A	21.1272	8.12521	-1.49546	0.000179
ARNT2	1.08718	0.416799	-1.5	0.021107
MUC21	27.0311	10.3626	-1.50007	0.000142
SERPINA12	10.0417	3.82449	-1.50951	0.001381
CCBP2	1.63925	0.622782	-1.51307	0.040646
RAPGEF3	1.14625	0.439459	-1.51377	0.020679
CEACAM6	94.2063	35.6128	-1.52027	0.000251
SEMA7A	4.99729	1.96415	-1.52188	0.002253
SHF	9.78356	3.68687	-1.5248	0.000803
CEACAM7	13.8434	5.19308	-1.53138	0.000416
LGALS1	180.302	67.5538	-1.53314	0.000102
CTSL2	66.0985	24.758	-1.53416	0.000302
KRT80	157.066	58.3824	-1.54012	0.0013
CLEC2B	3.0125	1.12287	-1.54061	0.024653
ECM1	256.631	94.7383	-1.54175	0.00093
MLPH	1.80645	0.674938	-1.55281	0.020929
KLK14	4.71958	1.73925	-1.55703	0.030191
MIR210HG	4.42877	1.6285	-1.5602	0.007271
ESYT3	2.80571	1.02919	-1.5637	0.004155
3-Mar	2.94486	1.07584	-1.56958	0.004315
RNF39	19.5417	7.22099	-1.57091	0.000187
GPR111	2.62724	0.954864	-1.57702	0.003123
SPTBN5	0.44769	0.162672	-1.57737	0.029351
ZNF555	2.06264	0.75378	-1.58822	0.00132
SLC6A14	20.5034	7.38176	-1.59067	5.75E-05
SERPINB9	4.84382	1.73085	-1.6015	0.000816
SLC26A9	4.24966	1.55532	-1.6015	0.000816
SPRR2F	27.4731	9.78694	-1.60593	0.001105
EMP3	13.6173	4.83076	-1.61195	0.004343
SLC5A1	19.0366	6.73827	-1.61628	4.39E-05
SDR9C7	21.8245	7.70723	-1.6185	0.000132
SLC13A4	1.64241	0.57109	-1.64087	0.029154

PSAPL1	8.71749	3.02892	-1.64194	9.47E-05
NPR2	2.20855	0.769098	-1.64672	0.010917
HCG22	3.35319	1.15474	-1.65481	0.000682
CST6	46.1786	15.8656	-1.65816	0.000202
LINC00319	1.91319	0.656418	-1.66013	0.019003
ADRB2	6.93458	2.36585	-1.66829	0.001631
KRT15	325.81	110.793	-1.67301	0.000452
PGLYRP4	79.4136	26.8069	-1.68362	2.48E-05
VSIG10L	46.2237	15.4332	-1.69944	2.46E-05
FAM25A	67.8396	22.4766	-1.71054	0.000201
C21orf7	1.63799	0.541671	-1.71327	0.046707
HSPB8	9.24948	3.04815	-1.71828	0.00049
LCE2A	59.0463	19.4351	-1.72002	6.77E-05
AGAP11	2.52904	0.828227	-1.72072	0.007186
HYAL1	5.38962	1.68809	-1.73081	0.00257
CNFN	721.862	235.606	-1.73218	8.08E-05
LGALS9B	3.34594	1.07393	-1.75634	0.027117
C7orf57	3.04559	1.0273	-1.75634	0.011893
IFI6	8.68132	2.84889	-1.75634	0.008246
BDKRB1	6.01298	1.90553	-1.77472	0.005993
TCN1	4.48672	1.4198	-1.77681	0.007916
FCHSD1	21.9994	6.9484	-1.77909	7.66E-06
SMPD3	24.6573	7.74526	-1.78747	7.27E-06
FGD2	1.39837	0.438391	-1.79029	0.023567
CRISP3	5.88265	1.83092	-1.80074	0.001026
XKRX	7.95386	2.47489	-1.80113	0.000133
ATG9B	23.2719	7.24138	-1.80132	5.86E-06
CSPG4	0.716699	0.222368	-1.80525	0.010854
PTCD1	3.72798	1.15905	-1.80597	0.000186
IL36RN	34.2847	10.6961	-1.81317	5.30E-06
SPRR2C	35.6369	10.9695	-1.81672	9.38E-05
MMP2	5.50197	1.69338	-1.82452	0.000205
RNASE7	124.077	37.8939	-1.82804	6.79E-06
KLK6	11.6747	3.60692	-1.83077	0.000273
C18orf26	1.85639	0.56448	-1.83435	0.02679
ZNF365	4.17548	1.24415	-1.84488	0.000319
TGM5	9.61207	2.80098	-1.84871	5.95E-05
SERPINE1	38.9626	11.7549	-1.85007	3.46E-06
LIPM	29.2906	8.81263	-1.85165	1.14E-05
RNF223	8.20786	2.43616	-1.86924	0.002448
GDA	5.94488	2.17955	-1.87109	2.20E-05
IL23A	2.47085	0.732054	-1.87182	0.049354

FN1	27.64	8.17514	-1.88108	5.43E-06
NKPD1	7.52134	2.21066	-1.88335	1.51E-05
DLX2	2.53577	0.744922	-1.8841	0.008628
CXCR7	8.3463	2.45186	-1.8841	0.0002
IL1R2	3.08575	0.920779	-1.89385	0.016743
TMEM132B	0.378951	0.109048	-1.91388	0.037156
LCE2B	156.558	44.944	-1.91734	1.58E-06
RHBG	1.49563	0.466034	-1.92627	0.041236
GPSM1	12.1397	3.21886	-1.92714	6.38E-06
FLG	47.8845	13.589	-1.93395	5.26E-05
SCNN1D	1.17016	0.343151	-1.93692	0.025845
LCE1A	198.523	56.1421	-1.93899	1.23E-06
LCE1C	117.831	33.0181	-1.95223	1.18E-06
LCE1B	68.3343	19.1426	-1.95266	1.24E-06
S100A6	567.321	158.126	-1.95993	8.86E-06
GSDMA	67.9073	18.5941	-1.98556	7.94E-07
LOXL2	2.57306	0.700711	-2.0135	0.001041
EGFL8	3.67043	1.06475	-2.01938	0.009366
ST6GALNAC1	3.46428	0.924515	-2.02262	0.001429
KCTD4	5.18719	1.37993	-2.0272	0.000595
COX6B2	1.72681	0.458689	-2.02936	0.028748
ABCG4	2.162	0.598133	-2.04392	0.001671
ELMOD1	4.00286	1.0624	-2.04852	0.000383
FGF5	0.513723	0.144004	-2.0518	0.031587
CASP14	16.315	4.24587	-2.05891	8.41E-07
ALDH3A1	16.1135	4.18195	-2.06589	5.90E-06
LCE2D	93.3328	24.0071	-2.07576	5.34E-07
IGLON5	0.79858	0.205054	-2.07827	0.034776
SLC47A2	6.67977	1.75362	-2.08299	0.000104
KIAA1644	0.998906	0.254606	-2.08892	0.002732
SULT1B1	3.63113	0.922664	-2.09338	0.007449
CHRNA9	2.65398	0.670299	-2.10212	0.003647
USP2	5.23575	1.45218	-2.10568	3.45E-05
DHRS9	27.3434	6.86805	-2.11069	7.34E-07
ACSBG1	1.23198	0.320613	-2.11891	0.014395
CXCL14	105.699	26.3868	-2.11891	2.73E-07
DSC1	9.08248	2.29473	-2.12157	1.09E-06
IGFBP6	14.5563	3.61922	-2.12473	0.000115
TMEM86A	21.1973	5.26239	-2.12809	1.60E-07
MSH5-SAPCD1	0.972757	0.235653	-2.13486	0.011337
PSG2	1.29001	0.315467	-2.14866	0.042388
LCE6A	84.9878	20.3968	-2.17575	1.91E-07

ENDOU	18.9507	4.59805	-2.17999	3.53E-07
MT2A	203.72	48.699	-2.18146	7.05E-08
CYP4F22	12.3353	2.94809	-2.18178	1.23E-06
DNASE1L2	2.01632	0.479387	-2.1893	0.023534
CHI3L1	5.98348	1.41874	-2.19321	0.000249
HYAL4	2.0167	0.475561	-2.20113	0.005011
NDUFA4L2	5.91809	1.39119	-2.20565	0.001491
NPR3	0.607935	0.144264	-2.21578	0.006529
CCL24	6.05146	1.41259	-2.21578	0.034239
CFTR	0.403784	0.0933127	-2.23027	0.025522
LCE2C	101.124	23.2283	-2.23901	6.38E-08
KCNE1	0.877545	0.209704	-2.24177	0.019355
LCE1F	146.714	32.8463	-2.27604	2.05E-08
EGR3	8.70421	1.94984	-2.28181	2.28E-07
DKK1	1.42638	0.316953	-2.28686	0.020813
ENO2	1.30779	0.288582	-2.29691	0.012338
ADAMTS1	10.2196	2.25511	-2.29691	7.51E-08
IGFL1	138.427	30.1714	-2.31471	1.05E-08
TREX2	7.57473	1.57017	-2.38711	0.000185
LCE1D	65.8624	13.6003	-2.39265	3.07E-07
PLA2G4B	40.2165	8.30458	-2.39291	3.65E-09
FRY	0.323396	0.0652453	-2.4262	0.007011
PLA2G4D	2.98398	0.585296	-2.46684	6.65E-05
MXRA5	6.40136	1.2529	-2.46995	3.56E-09
KCNMA1	1.7114	0.337059	-2.47059	7.61E-05
TNFRSF6B	2.01445	0.402936	-2.47255	0.019084
BPIFC	11.3027	2.1831	-2.48906	5.53E-07
HAL	4.9103	0.960323	-2.49082	1.56E-06
KIF26A	0.2931	0.0564452	-2.49331	0.025404
ZNF662	4.5797	0.861328	-2.51964	1.76E-07
RTN1	1.04577	0.223707	-2.52188	0.034496
IGFL3	11.3683	2.11249	-2.54484	0.000275
MMP1	5.088	0.967246	-2.5637	6.87E-05
S100A4	4.25436	0.868585	-2.5637	0.020033
MMP9	1.78039	0.326541	-2.5637	0.00271
PCDHGA5	0.307647	0.0608375	-2.5637	0.048024
LCE5A	3.38543	0.62092	-2.5637	0.009517
MPP2	0.493773	0.0864461	-2.63081	0.015806
NGEF	0.563221	0.11282	-2.66323	0.036488
SLC16A6	0.516864	0.0989214	-2.68234	0.020781
FCHO1	0.908266	0.166263	-2.70388	0.007798
TIAF1	1.36314	0.220365	-2.75634	0.006241

PRB2	1.10951	0.178058	-2.75634	0.02776
RGCC	2.14492	0.344224	-2.75634	0.009855
AQP9	0.524456	0.0841664	-2.75634	0.02776
PTGER3	1.98846	0.36334	-2.77804	2.74E-06
LCE1E	33.5119	5.17591	-2.81163	4.98E-10
MEF2B	1.19178	0.208542	-2.84381	0.021148
KLHL6	0.203688	0.0301741	-2.87182	0.037763
LOR	80.7339	11.741	-2.89846	3.00E-12
CCL22	1.66284	0.239628	-2.91162	0.000509
CYP26B1	0.787292	0.112309	-2.92627	0.001752
IGSF22	0.433619	0.0617884	-2.92627	0.016133
MMP10	2.81478	0.397518	-2.94077	0.000423
IVL	71.659	9.91461	-2.97036	9.68E-13
NR4A1	0.586822	0.100288	-2.97874	0.02802
KCNN4	0.839935	0.113512	-3.00427	0.012324
PSG7	5.98116	0.836074	-3.00788	6.18E-06
KRT37	3.91945	0.518005	-3.03645	6.30E-05
KPRP	124.81	16.2759	-3.05576	3.66E-12
PSG5	1.00735	0.161457	-3.07827	0.02084
MMP3	2.7627	0.347739	-3.10684	0.000224
PAPL	20.6342	2.55469	-3.13065	6.05E-13
EPHA8	2.98593	0.322206	-3.15489	9.70E-05
CYP4F2	1.59445	0.188545	-3.19692	0.000693
FRMPD1	2.41718	0.284472	-3.2038	4.98E-07
KLHL30	0.295594	0.0345002	-3.21578	0.037528
HLA-F-AS1	0.675554	0.0667367	-3.34131	0.026904
LOC100507564	1.01634	0.116087	-3.34131	0.026904
STEAP1B	1.06805	0.0979456	-3.45678	0.019374
APOD	2.80422	0.225015	-3.75634	0.00042
SCNN1G	0.735816	0.0545013	-3.87182	0.00092
C1orf68	11.451	0.840088	-3.88563	4.39E-08
GPBAR1	0.603274	0.0915109	-3.92627	0.034093
MYO1H	0.209304	0.0149288	-3.92627	0.034093
POU5F1	0.622654	0.0730543	-3.92627	0.034093
ARC	0.302825	0.0215993	-3.92627	0.034093
FAM65C	0.855848	0.0593942	-3.9658	0.000121
GP1BB	2.08565	0.136895	-4.07827	0.002148
FOSB	0.296567	0.0340534	-4.07827	0.023276
MYPN	0.204422	0.0221812	-4.07827	0.023276
LOC149086	0.847807	0.0544235	-4.07827	0.023276
HNRNPH2	8.45215	0.542771	-4.10684	1.90E-12
GYS2	0.347785	0.0202959	-4.21578	0.016015

ARG1	5.60549	0.257025	-4.5637	2.61E-08
SYNPO2L	0.623297	0.0387408	-4.66323	0.000116
FSBP	0.355492	0.0171707	-5.00427	0.000995
AQP5	3.15397	0.104723	-5.02936	3.05E-07
CAPN8	0.989767	0.0302554	-5.14866	0.000518
C4orf26	0.374112	0	-6.30345	0.038212
LY75	0.0989903	0	-6.30345	0.038212
RELN	0.0513609	0	-6.30345	0.038212
IFNK	0.521178	0	-6.30345	0.038212
SYT14L	0.263222	0	-6.30345	0.038212
MYCBPAP	0.217294	0	-6.52323	0.023764
CACNA1D	0.116176	0	-6.71391	0.015043
CCL20	0.942526	0	-6.71391	0.015043
NPPA-AS1	0.497653	0	-6.71391	0.015043
C1orf177	0.557644	0	-6.88231	0.009667
NWD1	0.129528	0	-7.03309	0.006294
KRTAP5-4	0.838475	0	-7.03309	0.006294
XCR1	1.02833	0	-7.29428	0.002758
CA9	0.764663	0	-7.29428	0.002758
SEN3-EIF4A1	0.293999	0	-7.29428	0.002758
C9orf131	0.489218	0	-7.51536	0.001255
ZNF321P	0.678821	0	-7.61437	0.000856
PTPN5	0.54883	0	-7.70702	0.000589
SLC6A2	0.649817	0	-7.95386	0.000198
UBE2F-SCLY	1.60147	0	-9.28737	2.64E-08
MUTED	2.36062	0	-9.63266	8.66E-10
PALM2-AKAP2	0.984738	0	-9.91105	3.59E-11
TMX2-CTNND1	1.51256	0	-10.2711	2.87E-13

Supplemental Table S2. GO: Molecular Function

ID	Name	pValue	Genes from Input	Genes in Annotation
1	GO:0005509 calcium ion binding	5.388E-7	45	708
2	GO:0038024 cargo receptor activity	7.485E-7	12	71
3	GO:0008236 serine-type peptidase activity	1.986E-6	22	242
4	GO:0017171 serine hydrolase activity	2.435E-6	22	245
5	GO:0004252 serine-type endopeptidase activity	4.074E-6	20	215
6	GO:0005044 scavenger receptor activity	6.312E-6	9	47
7	GO:0004175 endopeptidase activity	2.395E-5	30	457
8	GO:0015291 secondary active transmembrane transporter activity	5.357E-5	19	236
9	GO:0042802 identical protein binding	5.841E-5	64	1359
10	GO:0005125 cytokine activity	7.640E-5	18	222
11	GO:0002020 protease binding	1.151E-4	12	115
12	GO:0016638 oxidoreductase activity, acting on the CH-NH2 group of donors	1.584E-4	5	19
13	GO:0019955 cytokine binding	1.790E-4	11	103
14	GO:0005518 collagen binding	2.090E-4	9	72
15	GO:0015075 ion transmembrane transporter activity	2.108E-4	44	873

GO: Biological Process

ID	Name	pValue	Genes from Input	Genes in Annotation
1	GO:0018149 peptide cross-linking	3.322E-21	23	57
2	GO:0031424 keratinization	1.154E-20	22	53
3	GO:0008544 epidermis development	2.465E-20	48	340
4	GO:0043588 skin development	7.283E-20	43	278
5	GO:0030216 keratinocyte differentiation	1.824E-18	30	138
6	GO:0009913 epidermal cell differentiation	1.631E-15	32	200
7	GO:0016477 cell migration	4.759E-12	82	1300
8	GO:0040011 locomotion	7.712E-12	99	1735
9	GO:0060429 epithelium development	1.047E-11	81	1296
10	GO:1901700 response to oxygen-containing compound	2.252E-11	93	1614
11	GO:0006954 inflammatory response	3.784E-10	52	711
12	GO:0051674 localization of cell	5.066E-10	82	1428
13	GO:0048870 cell motility	5.066E-10	82	1428
14	GO:0030334 regulation of cell migration	5.906E-10	53	742
15	GO:1902533 positive regulation of intracellular signal transduction	9.700E-10	62	958

GO: Pathway

ID	Name	P Value	Genes from Input	Genes in Annotation
1	1457791 Formation of the cornified envelope	1.343E-22	27	71
2	M5889 Ensemble of genes encoding extracellular matrix and extracellular matrix-associated proteins	9.224E-18	87	1028
3	1457790 Keratinization	1.006E-15	35	214
4	M5885 Ensemble of genes encoding ECM-associated proteins including ECM-affiliated proteins, ECM regulators and secreted factors	2.839E-15	68	753
5	1470923 Interleukin-4 and 13 signaling	1.916E-8	18	114
6	M3468 Genes encoding enzymes and their regulators involved in the remodeling of the extracellular matrix	4.142E-8	26	238
7	1270302 Developmental Biology	1.709E-6	63	1081

8	M5883	Genes encoding secreted soluble factors	1.786E-6	29	344
9	1269310	Cytokine Signaling in Immune system	4.550E-6	48	763
10	1269318	Signaling by Interleukins	6.491E-6	37	531
11	169349	Validated transcriptional targets of AP1 family members Fra1 and Fra2	8.732E-6	8	34
12	M3008	Genes encoding structural ECM glycoproteins	1.623E-5	19	196
13	PW:0000051	histidine metabolic	4.113E-4	4	12
14	83051	Cytokine-cytokine receptor interaction	4.145E-4	20	270
15	1268755	Regulation of Insulin-like Growth Factor (IGF) transport and uptake by Insulin-like Growth Factor Binding Proteins (IGFBPs)	4.287E-4	5	21

Supplemental Figure S1. Demographics of patient cohorts examined in RNAseq analysis or qPCR.

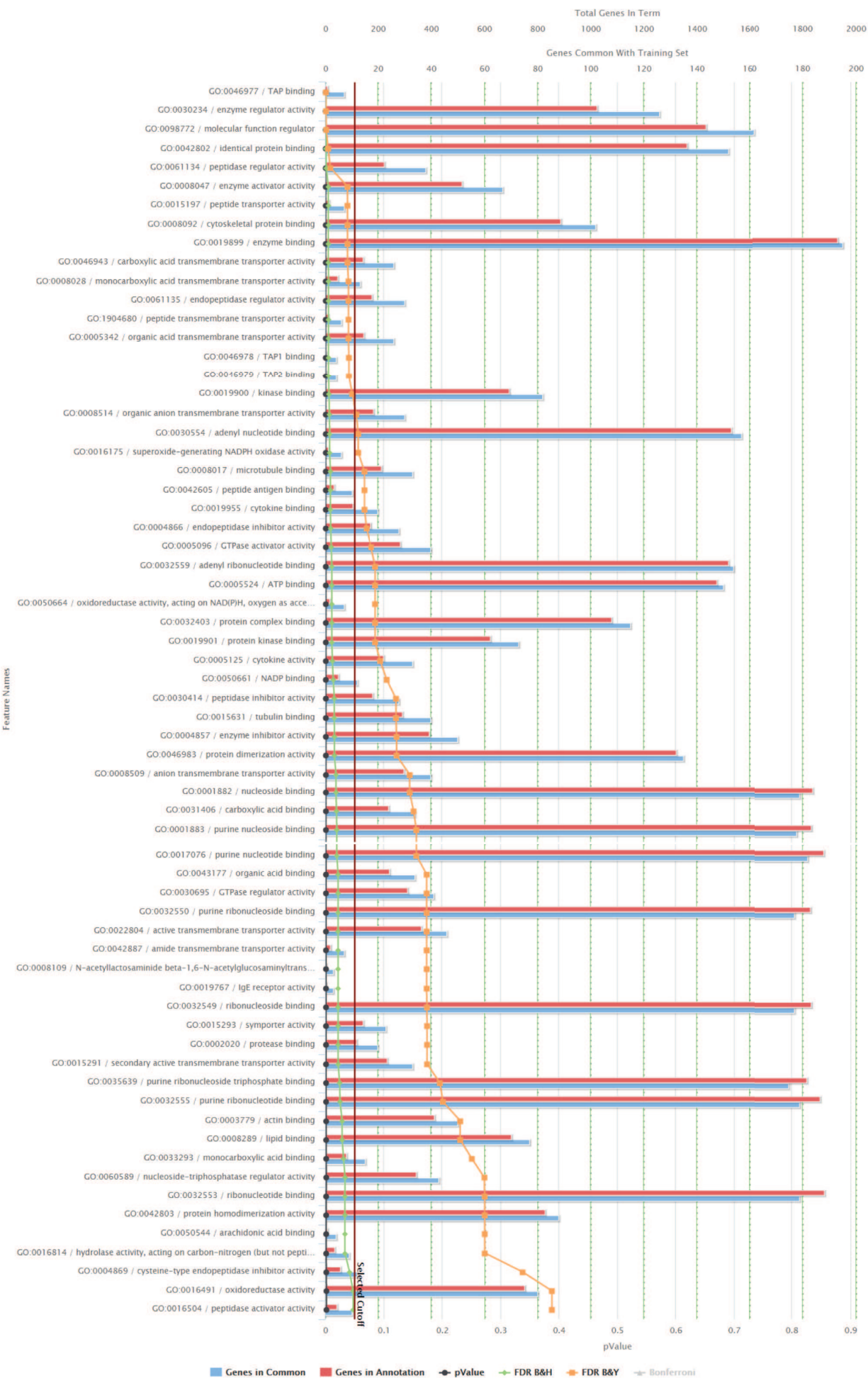
Biopsy set 1 (Cohort 1): RNAseq cohort (NL=6, EoE=10)

	Age	Male	Female	Max Eosinophils per high powered field (hpf)
<i>NL</i>	12.7 ± 6.0	50%	50%	0 ± 0
<i>EoE</i>	15.1 ± 12.4	60%	40%	163.6 ± 92.4

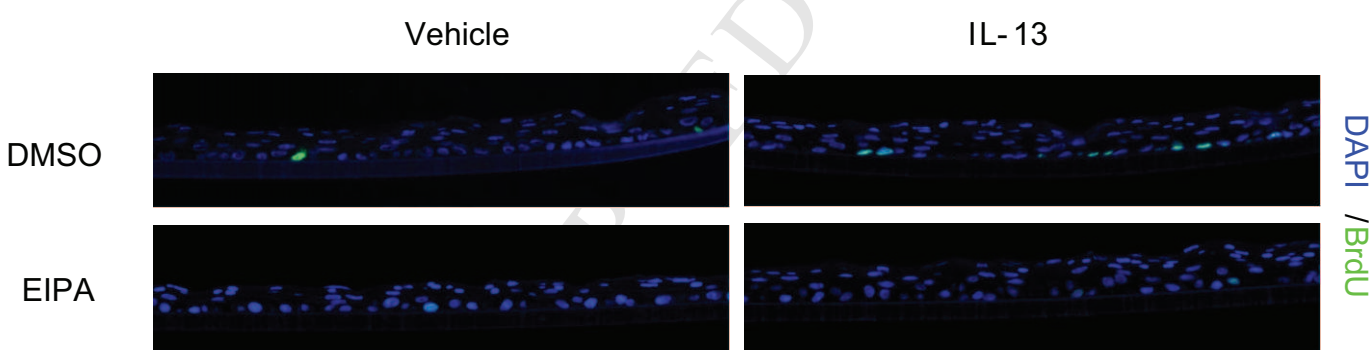
Biopsy set 2 (Cohort 2): qPCR cohort (NL=10, EoE=10)

	Age	Male	Female	Max Eosinophils per high powered field (hpf)
<i>NL</i>	9.7 ± 3.1	50%	50%	0 ± 0
<i>EoE</i>	10.7 ± 5.3	80%	20%	124.4 ± 73.5

Significant Terms For: GO: Molecular Function



(A).



(B).

